We are IntechOpen, the world's leading publisher of Open Access books Built by scientists, for scientists

6,900
Open access books available

186,000
International authors and editors

200M
Downloads

Our authors are among the

154
Countries delivered to

TOP 1%
most cited scientists

12.2%
Contributors from top 500 universities

CLARIVATE ANALYTICS
BOOK CITATION INDEX
INDEXED

WEB OF SCIENCE™

Selection of our books indexed in the Book Citation Index
in Web of Science™ Core Collection (BKCI)

Interested in publishing with us?
Contact book.department@intechopen.com

Numbers displayed above are based on latest data collected.
For more information visit www.intechopen.com

Silicon Nanocluster in Silicon Dioxide: Cathodoluminescence, Energy Dispersive X-Ray Analysis and Infrared Spectroscopy Studies

Roushdey Salh

Institute of Physics, Faculty of Science and Technology, Umeå University, Umeå
Sweden

1. Introduction

This chapter is extended to various electronical and optical modifications of amorphous silica (a-SiO_2) layers as they are applied in microelectronics, optoelectronics, as well as in the forthcoming photonics. Scanning electron microscopy (SEM), energy dispersive X-ray analysis (EDX), Fourier transform infrared spectroscopy (FTIR) and cathodoluminescence (CL) have been used to investigate thermally grown pure amorphous silicon dioxide and ion-implanted layers with thickness d_{ox}=100-500 nm. The main luminescent centers in silicon dioxide layers are the red luminescence (650 nm; 1.85 eV) of the non-bridging oxygen hole center (NBOHC; $\equiv$Si–O$\bullet$), a blue (460 nm; 2.7 eV) and a ultra violet luminescence (290 nm; 4.3 eV) of the oxygen deficient centers (ODC's; $\equiv$Si$\cdots$Si$\equiv$), and a yellow luminescence (570 nm; 2.2 eV) appears especially in hydrogen treated silica indicating water molecules, and on the other hand, in silicon excess samples indicating higher silicon aggregates. A quite different CL dose behavior of the red luminescence is observed in dry and hydrogen-treated samples due to dissociation and re-association of mobile hydrogen and oxygen to radicals of the silica network. Additionally implanted hydrogen diminishes the red luminescence in wet oxide but maintains the blue and the UV bands. Thus hydrogen passivates the NBOHC and keeps the ODC's in active emission states. A model of luminescence center transformation is proposed based on radiolytic dissociation and re-association of mobile oxygen and hydrogen at the centers as well as formation of interstitial H_2, O_2, and H_2O molecules.

Non-stoichiometric SiO_x layers produced by direct ion implantation or reactive sputtering are used to investigate whether the different luminescent centers are related to oxygen or to silicon. Oxygen implantation as well as direct silicon implantation led to an oxygen surplus as well as an oxygen deficit, respectively. The related luminescence damages provide direct evidence to the nature of the defects. Oxygen-deficient thin silica layers SiO_x with different stoichiometric degree $1 \leq x \leq 2$, were prepared by thermal evaporation of silicon monoxide in vacuum and in ambient oxygen atmosphere of varying pressure onto crystalline silicon substrates. The chemical composition has been calibrated and determined by FTIR spectroscopy. The CL spectra of the oxygen-deficient layers shows the development of typical silica luminescence bands at the composition threshold $x \leq 1.5$ onwards to x=2. The

green-yellow luminescence (2.15 eV) strongly increases with the annealing temperature up to 1300 °C which is attributed to the formation of small silicon aggregates in the network, from dimers over trimers even to hexamer rings.

Ion implantation doses between 3×10^{16} and 5×10^{16} ions/cm² led to an atomic dopant fraction of about 4 at.% at the half depth of the SiO_2 layers. In ion implanted SiO_2 layers additional emission bands are observed. A huge violet band in Ge^+ implanted layers appears at λ=410 nm (3.1 eV). This band corresponds to the Ge-related oxygen deficient center (Ge-ODC). The thermal annealing process of the Ge^+ implanted layers leads first to a strong increase of the violet luminescence due to formation of Ge dimers, trimers or higher aggregates, finally to destruction of the luminescence centers by further growing to Ge nanoclusters. Scanning transmission electron microscopy (STEM) shows the growing in Ge cluster size with increasing annealing temperature up to 1100 °C. As a result of ion implantation, we can state that; group IV elements (C, Si, Ge, Sn, Pb) in SiO_2 increase the intensity of the luminescence in the blue region and group VI elements (O, S, Se) increase the intensity in the red region, confirming the association of the defect centers in the blue and the red region with oxygen deficient centers and oxygen excess centers, respectively. The cathodoluminescence spectra of sulfur-implanted SiO_2 layers and oxygen implanted layers under special conditions show besides the characteristic luminescence bands a multimodal structure beginning in the green region at 500 nm over the yellow-red region and extending to the near IR measured up to 820 nm. The energy step differences of the sublevels amount to an average 120 meV and indicate vibronic-electronic transitions, probably of O^-_2 interstitial molecules, which could be demonstrated by a respective configuration coordinate model.

2. CL of stoichiometric and non-stoichiometric SiO_2

2.1 Wet and dry SiO_2 layers

The CL spectra of pure SiO_2 consist of several broad bands and certainly of some overlapped components especially at the region around $\lambda \approx$ 460-620 nm (2.7-2.0 eV). The irradiation response of these luminescence bands indicates that they are associated with different defect centers. Even at specimen temperatures as low as LNT where thermal contributions to the bandwidth are almost minimized, the SiO_2 CL emission bands are still broad because of the degree of coupling between the host lattice and the defects associated with the luminescence emissions [Griscom 1990b].

The initial (1 sec) and the saturated (5 h) CL spectra of pure SiO_2 layers are presented in Fig. 2.1. The main CL emission bands in wet and dry specimens at temperatures between liquid nitrogen (LNT) and room temperature (RT) are the red luminescence R at 650 nm (1.9 eV) associated with the NBOHC [Fitting et al. 2005b], the blue B and ultraviolet UV bands at 460nm (2.7 eV) and 290 nm (4.3 eV) respectively, associated with the Si related oxygen deficient center (Si-ODC) [Skuja 1994b]. Some shoulders can be also seen in the green-yellow G-Y region between 500-580 nm (2.5-2.1 eV). A luminescence band at 500 nm (2.5 eV) in crystalline SiO_2 and another at 560 nm (2.2 eV) in amorphous SiO_2 is often ascribed to the self trapped exciton (STE) [Skuja et al. 1978, Trukhin et al. 1998]. Another CL band which is not often discussed in the literature is easily seen in the yellow Y region at $\lambda \approx$570-580 nm (2.18-2.14 eV) especially at LNT, but it is also expected in RT spectra where the plane between the B band and the R bands can accommodate more than one overlapped emission band.
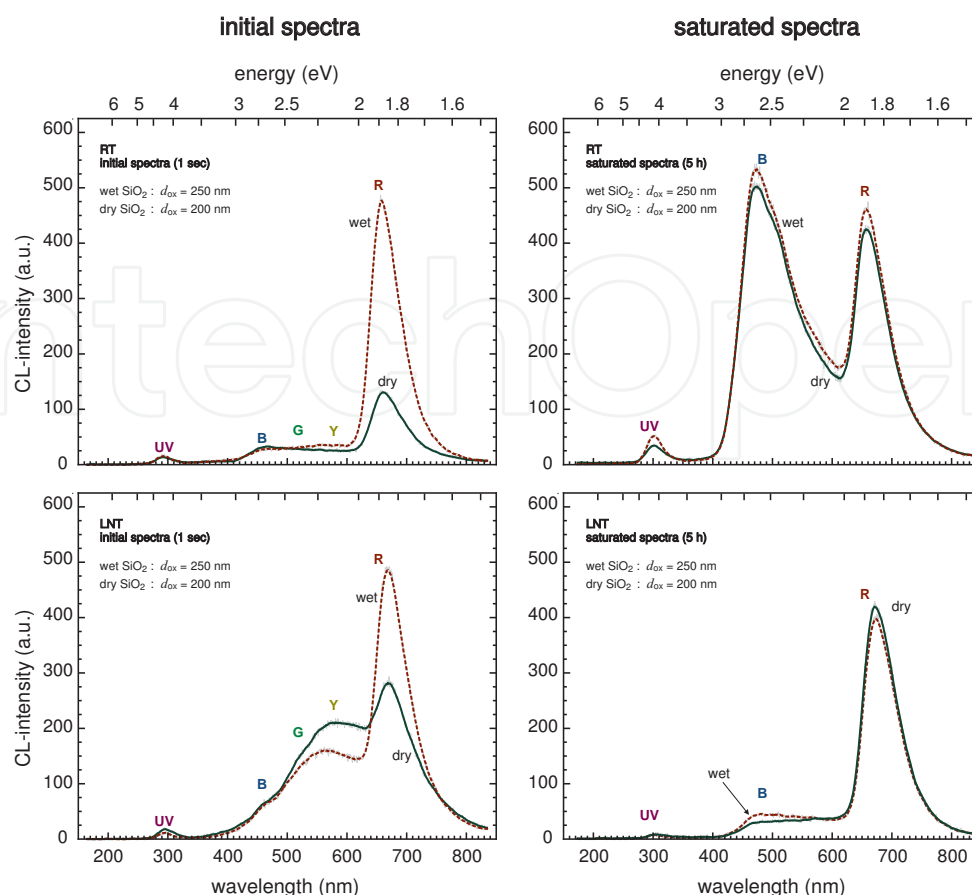
Silicon Nanocluster in Silicon Dioxide: Cathodoluminescence,
Energy Dispersive X-Ray Analysis and Infrared Spectroscopy Studies

175

Fig. 2.1 The initial (1sec) and saturated (5h) CL spectra of wet and dry SiO_2 at room temperature (RT) and liquid nitrogen temperature (LNT); electron beam energy E_o=10 keV and current density j_o=5.4 mA/cm².

CL bands in this region will be discussed in more detail in the following sections. Based on our basic experimental observations we presume a very thin ice (H_2O) layer to have been produced on the surface of the sample as an effect of low temperatures which could be one of the reasons for the Y band, but under any circumstances one can see that the local intrinsic defects like ODC and NBOHC dominates the CL spectrum at LNT too.

Looking to the 1 sec spectra of both wet and dry SiO_2 in Fig. 2.1, we can state that some of the detected luminescence bands have the same origin and they behave similarly under electron beam irradiation but others are totally different or are formed/transformed by more complex reactions. The UV luminescence always peaks at very low intensities which scarcely change under irradiation. This band was not detected in many crystalline SiO_2 modifications at room temperature even or at liquid nitrogen temperature [Barfels 2001] but it is clearly seen in bulk and thin layers of amorphous SiO_2 [Trukhin et al. 1998, Bakaleinikov et al. 2004]. Absence of the crystalline order seems to be the origin of the UV luminescence band. The blue B luminescence starts with the same intensity in both dry and wet at RT and LNT and reaches the saturation level (5 h) together. The B band grows drastically during the irradiation at room temperature (RT), while it is expected that a high energetic electron beam creates more oxygen vacancy or in other words oxygen deficient centers (ODC).

The main difference between the CL spectra of wet and dry SiO_2 is located in the Y and R region. The Y luminescence is detected with relatively higher intensity in wet SiO_2 at RT and

it is more visible at LNT in both dry and wet SiO_2 which is probably associated with some crystalline H_2O molecules on the sample surface. A considerable increase in the R band intensity is clearly seen in the initial spectra in wet SiO_2. This is the main dissimilar point between dry and wet oxide layers. We suspect a direct connection of the Y and R bands with atomic or molecular hydrogen. The saturated spectra of wet and dry SiO_2 have almost the same profile, see Fig. 2.1. That means, the red luminescence is starting from different precursors in dry and wet SiO_2 and these precursors are destroyed or transformed to other similar structural defects in both kinds of layers during the electron irradiation.

2.2 Dose-temperature effect

It is well known that CL spectra of different SiO_2 modifications change during the initial period of excitation. The time evolution of the CL spectrum of wet and dry oxide a-SiO_2layers during electron irradiation at room temperature (RT) and liquid nitrogen temperature (LNT) is presented in Fig. 2.2. Comparison of time resolved bands shows clearly the increase of the initial CL intensity of the emission bands as the specimen temperature is reduced to LNT may be because of the reduction in the thermally assisted conversion of STE's to complementary defect pairs (oxygen deficient centers and oxygen excess centers) via nonradiative relaxation processes [Stevens-Kalceff 1998].
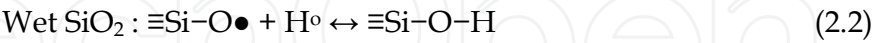
In Fig. 2.2 the amplitudes of the main luminescence peaks: red, R (650 nm, 1.85 eV), blue, B (460 nm, 2.7 eV), and UV (290 nm, 4.4 eV) have been recorded as a function of the irradiation time.

The UV band shows slightly increasing behavior for some 10 sec then stabilizing up to the saturation state. Using "track-stop" techniques [Fitting et al. 2004] it was possible to describe this band more comprehensively. The UV band is detected initially in the "track" mode followed by an increase at the beginning of the "stop" measurement, then a maximum (turnaround), decreasing and increasing again to a long term invariance, larger for the wet oxide than for the dry one.

The B band has a time dependence at LNT that differs from that at RT. Whereas it decreases at LNT for both the wet and the dry SiO_2, it increases from very low intensity for RT, i.e. it is fully generated during the irradiation process, probably from precursors like ODC centers [Fitting et al. 2002b]. The long term irradiation shows an increase to saturation even over several hours. The Y band has the same time dependence as the B band both at RT and LNT. It gives us an impression that both defect centers associated with the blue and the yellow luminescence are at least of the same kind, probably oxygen deficiency centers (ODC).

The most obvious difference in the luminescence of wet and dry oxides appears in the R dose dependence, Fig. 2.2 (top). Whereas the R luminescence of the wet oxide starts from an initial intensity, decreases to a minimum and then increases to a saturation, the red band dependence of the dry oxide differs: starting from a much lower intensity, increasing and approaching nearly the same saturation intensity as that of wet oxide. This is the main new finding for the different wet and dry oxides and therefore it will be discussed in more detail in dependence of other ion implantations, especially hydrogen which is the main key difference between the dry and wet oxide silicas. The red ($\approx$1.9 eV) luminescence is generally associated with NBOHC and attributed to the recombination of electrons in the highly localized nonbridging oxygen band gap state, with holes in the valence-band edge [Stevens-Kalceff 1998]. A remarkable difference in the dose behavior of the red peak in dry and wet specimens is found. This can be considered as a well recognized proof that the NBOHC

Silicon Nanocluster in Silicon Dioxide: Cathodoluminescence,
Energy Dispersive X-Ray Analysis and Infrared Spectroscopy Studies

177

defect structure of SiO_2 is extremely sensitive to hydrogen treatment which can result in the formation of defects and/or the formation of existing defect precursors in the presence of hydrogen atoms [Fitting et al. 2005a]. Other methods than CL have provided direct/indirect evidence for the existence of a number of different defect precursors for the NBOHC. Based on these facts, we may express two interactions where NBOHCs are involved;

$$\text{Dry } SiO_2 : \equiv Si-O\cdots Si \equiv \rightarrow \equiv Si-O\bullet + \bullet Si \equiv \tag{2.1}$$

$$\text{Wet } SiO_2 : \equiv Si-O\bullet + H^o \leftrightarrow \equiv Si-O-H \tag{2.2}$$
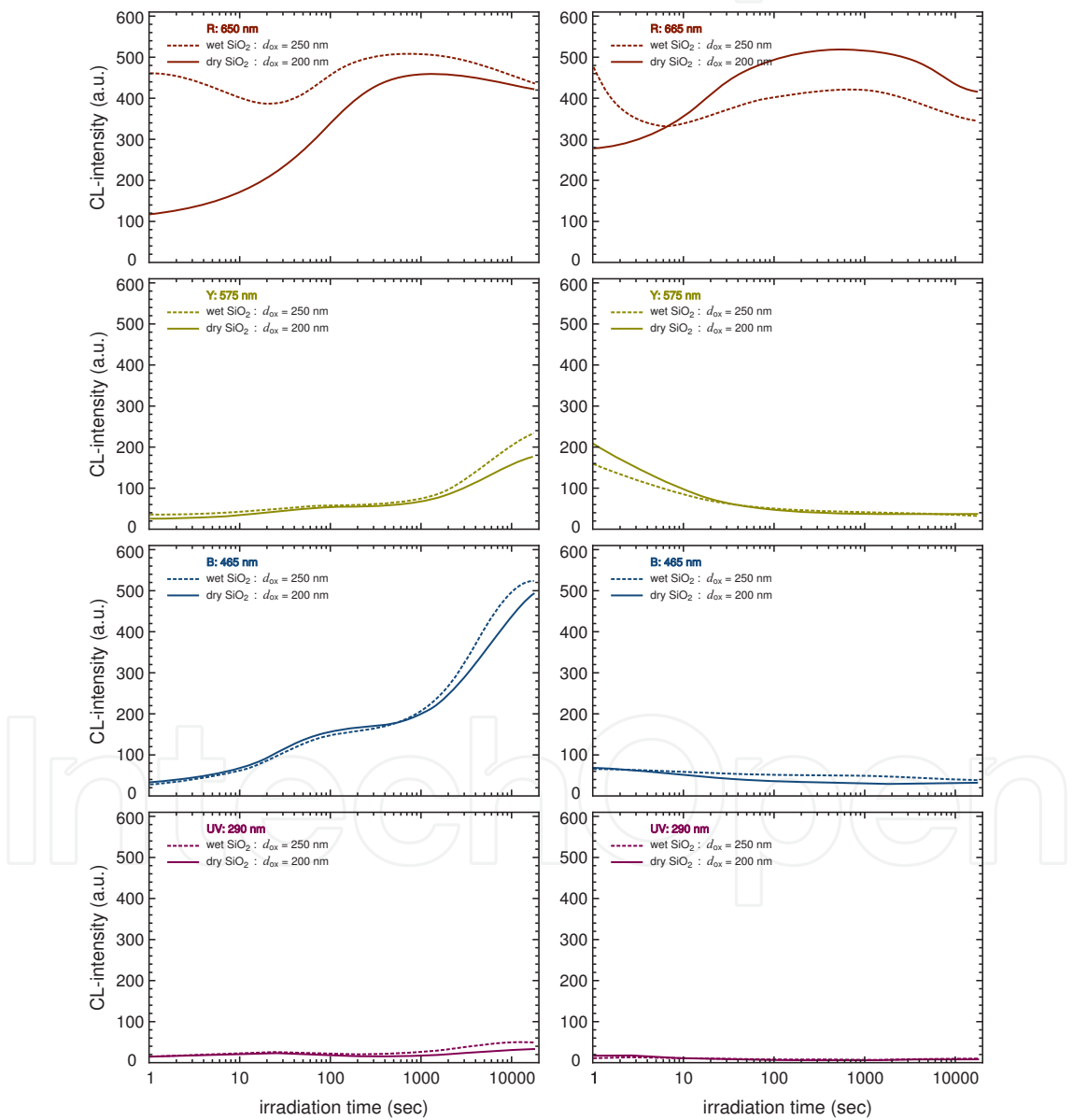
Fig. 2.2 CL dose dependencies of the red (R), the blue (B), the yellow (Y) and the ultraviolet (UV) bands in dry and wet SiO2 at room temperature (RT) and liquid nitrogen temperature (LNT); electron beam energy E_o=10 keV: current density j_o=5.4 mA/cm².

The most common production mode for the NBOHC in dry SiO_2 which contains a negligible amount of hydrogen and silanol groups, is by the strained bonds "···" between Si and O atoms, eq. (2.1), here both the $E´$-center and NBOHC can form in dry oxide layers. In wet SiO_2, hydrogen diffuses through the network and simultaneously undergoes reactions with the NBOHC during the first seconds of irradiation (destructive mode of NBOHC) followed by a slow creation mode [Tandon 2004]. This decay process is attributable to the simultaneous recombination of NBOHC with dissociated hydrogenous species, eq. (2.2). In wet SiO_2 layers, NBHOC are likely to react with interstitial molecular hydrogen at room temperature according to eq. (2.3).

$$\equiv Si−O\bullet + H_2 \rightarrow \equiv Si−O−H + H^o \tag{2.3}$$
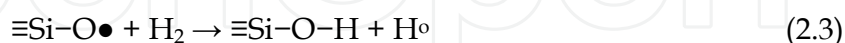
Both of these reactions of eqs. (2.2) and (2.3) reasonably explain the elimination of NBOHC in wet layers. Indeed, infrared (IR) measurements confirm that H^o or H_2 react with dangling bonds created by neutron irradiation [Bakos et al. 2004a]. But the most interesting point is that the formation and destruction mechanism of NBOHC has absolutely no dependence on a specimen's temperature because it is affected only by OH groups or hydrogen concentration, as is clearly shown with the red curves in Fig. 2.2.

In the dry SiO_2, the NBOHC defect concentration has the tendency to increase (creation) at both RT and LNT during the beginning of irradiation but it decreases in wet specimens (hydrogenated) due to interaction with the mobile hydrogen [Kajihara et al. 2002]. The intensity difference of NBOHC between the beginning and the end of electron irradiation is much less in wet SiO_2, which confirms the reliability of eqs. (2.1-2.3).

2.3 Lifetime measurement of the resolved CL bands

To identify whether the red bands in wet and dry oxide are due to the same electronic state we have measured their respective lifetimes. In Fig. 2.3 the pulsed luminescence of the red peak R (650 nm, 1.9 eV) is measured, and the red R luminescence decay with its lifetime, τ, is determined from the pulse switching-off decay (bottom). In the pulsed CL response we observe an increase and pumping of the luminescence over about 20 µs after switching on the electron beam. The overall pulse duration is 100 µs.

During this excitation the luminescence again decays very rapidly over about 30 µs to lower intensity. Of course, the first suggestion for such a change could be based on thermal quenching effects of the red luminescence due to electron beam heating of the irradiation spot on the sample. Indeed, the electron beam density with 0.1 A/cm² is about 20 times higher than that in the CL dose measurements in Figs. 2.1 and 2.2. However, this very rapid rise, turnaround, and decrease of the red luminescence at the beginning of the electron beam pulse may be discussed also in the context of Fig. 2.2 and in terms of center activation and destruction.

The red luminescence lifetime after switching-off the electron beam has been enlarged in the bottom of Fig. 2.3 showing a mean lifetime of about (4.7±0.2) µs for the wet oxide and (5.3±0.2) µs for the dry silicon dioxide layers, respectively. Thus we may state that the R luminescence lifetime in wet oxide is somewhat smaller than in dry oxide, but of the same order with τ~5 µs. However, the time dependence of the decay is not exponential, but a stretched exponential with (5≤τ≤20µs over longer decay ranges [Trukhin et al. 2003a]. The lifetime of the blue luminescence is measured too, in Fig. 2.4 the B band decay is indicating a rapid component with τ≈(50±8) µs as well as a slow one with τ≈(7.1±0.4) ms for the wet

Silicon Nanocluster in Silicon Dioxide: Cathodoluminescence,
Energy Dispersive X-Ray Analysis and Infrared Spectroscopy Studies

179

oxide, and $\tau \approx (70\pm2)$ µs as well as a slow one with $\tau \approx (7.8\pm0.8)$ ms for the dry oxide. Ultimately, the decay kinetics of the UV luminescence was measured by Goldberg [Goldberg 1996] at LNT and RT. The decaying process was found to be occurring over the first 5 ns followed by a hyperbolic one proportion to $t^{-1.5}$ in the µs range.
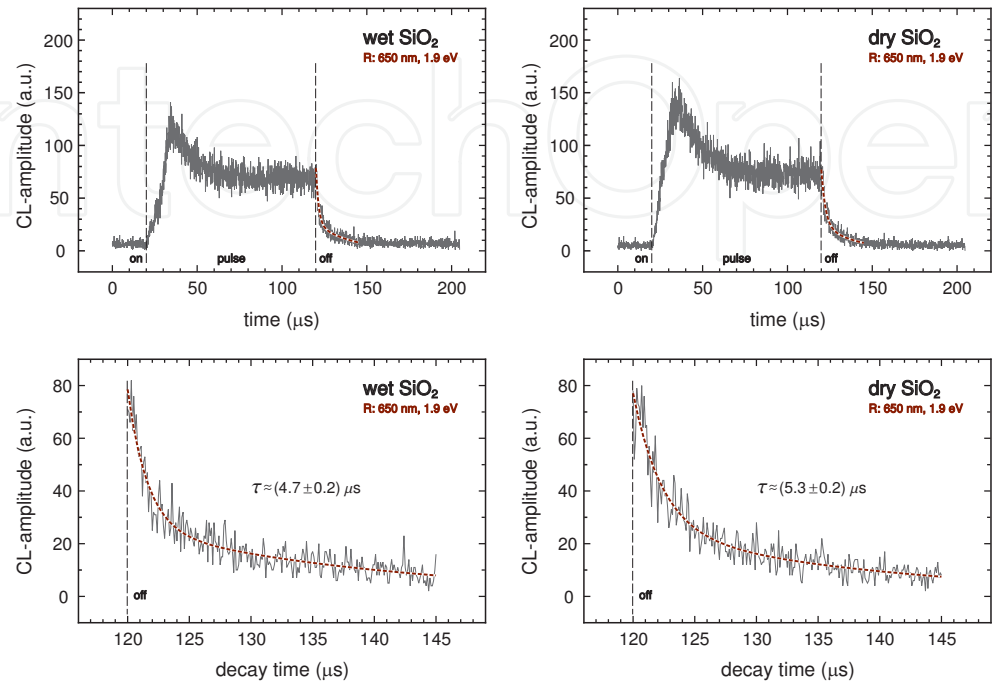

Fig. 2.3 CL pulsed excitation of the red R luminescence: 650 nm, 1.9 eV (top) with its temporary decay and lifetime τ (below) for wet (left) and dry (right) SiO_2 at RT; electron beam energy E_o=5 keV: current density j_o= 0.1 A/cm^2, [Fitting et al. 2005b].
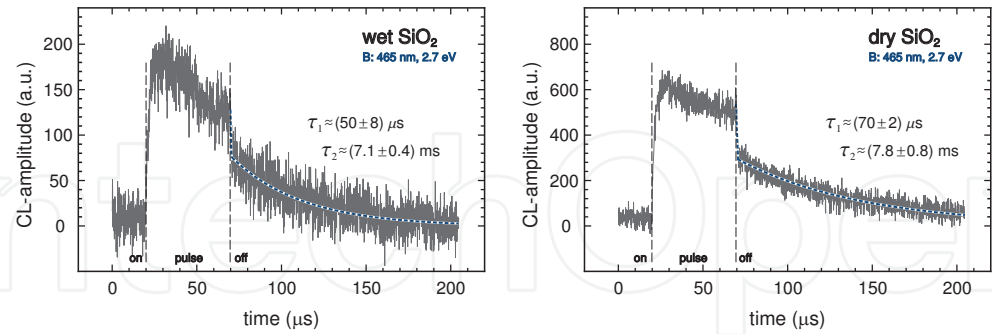
Fig. 2.4 CL pulsed excitation of the blue B luminescence: 465 nm, 2.7 eV with its temporary decay and lifetime τ for wet and dry SiO_2 at RT; E_o=5 keV: j_o= 0.1 A/cm^2.

2.4 Under-stoichiometric silica layers

The presence of intrinsic defects like oxygen vacancies or a presence of hydrogen atoms, plays an important role in numerous circumstances particularly in the growth of the layer structure. Thermal-annealing procedure leads to elimination of hydrogen and production of silicon nanoclusters in different sizes in silica network depending on the applied temperature. At annealing temperatures even below 900 °C, the hydrogen release from the

SiO$_x$ layers permits the formation of Si-O• radicals introducing structural disorder into the layer network [Fitting et al. 2005a]. At higher temperatures, the structure will undergo a network reaction similar to eq. (2.4), then giving rise to the formation of nanostructures.

$$SiOx \rightarrow (x/2)\, SiO_2 + (1-x/2)Si \qquad 1 \leq x \leq 2 \qquad (2.4)$$

In many cases cluster formation is affected by various kinds of defects in the Si-O network, which can be either crystalline or amorphous. Fourier transform infrared spectroscopy (FTIR) [Zacharias et al. 2003] and Cathodoluminescence (CL) [Fitting et al. 2002b] has been employed to characterize the silicon cluster growing and to study the effects of ionizing radiation on the structure of luminescent defects in SiO$_x$ systems [Trukhin and Fitting 1999, Trukhin et al. 1999]. The UV (4.3 eV), the blue (2.7 eV) and the red (1.9 eV) luminescence centers have been classified as process-induced centers, which also exist in irradiated SiO$_2$. Again the yellow luminescence band (2.15 eV) is distinguished more clearly in the SiO$_x$ layer, which we think deserves more attention and has to be studied intensively. In the present section, the annealing temperature dependence of the CL intensities of the 4.3, 2.7, 2.15 and 1.9 eV peaks and their correlation with the stoichiometry x will be demonstrated separately in order to associate the luminescence bands with the nature of different defects.

2.5 Fourier transform Infrared (FTIR) measurement of stoichiometric and under-stoichiometric silica layers

The vibrational spectrum of SiO$_2$ is full of details. It consists of longitudinal-optical (LO) and transversal-optical (TO) split features at around 460 cm^{-1}, 800 cm^{-1}, and 1100 cm^{-1}. The LO modes are not detected (lower frequencies) or only detected in oblique incidence IR transmission measurements. The highest frequency feature exhibits the largest absorption coefficient, therefore in the literature most attention is paid to this absorption band. In SiO$_2$ it features a TO absorption peak at around 1090 cm^{-1} with a LO absorption at around 1250cm^{-1}, being visible when applying oblique incident IR radiation. In the present work we focus on the region of the Si−O−Si stretching mode (700-1400 cm^{-1}).
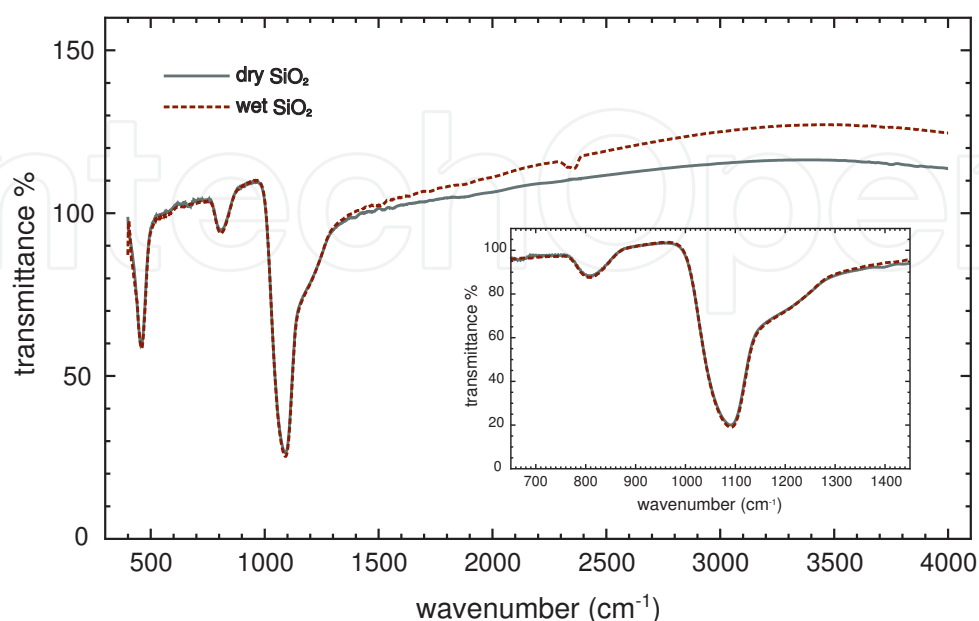

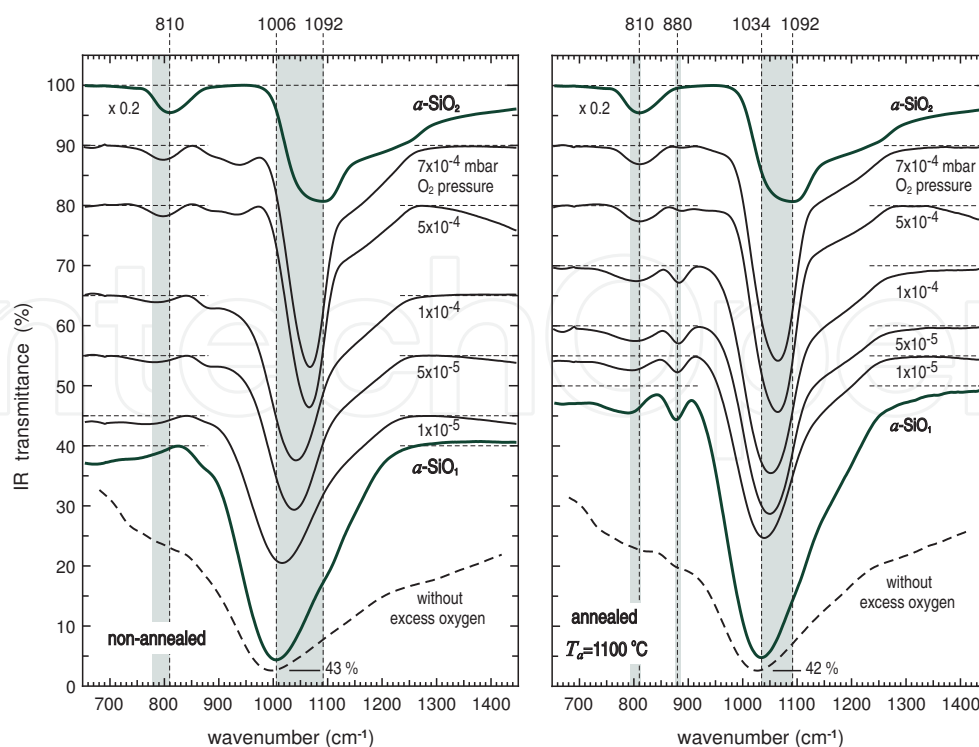Fig. 2.5 Fourier transform infrared (FTIR) spectra of thermally grown pure dry and wet SiO$_2$.

Fig. 2.6 Infrared spectra of SiO$_x$ layers on Si substrate grown by thermal evaporation of SiO in ambient oxygen pressures, the stoichiometric SiO$_1$ and SiO$_2$ layers are presented for calibration of non-annealed samples (left) and thermally annealed samples, T_a=1100 °C (right).

At first we present the IR spectra of thermally grown a-SiO$_2$ in Fig. 2.5, then a comparison of the non-annealed and the thermally annealed (T_a=1100 °C) silica layers with different stoichiometry x, before they have been irradiated (Fig. 2.6).

Typical IR transmittance spectra of wet and dry silica are presented in Fig. 2.5. Obviously there are no essential differences in spectra of silica samples with different thermal oxidization method (wet or dry). The only bands observed are due to the fundamental SiO$_2$ vibrational bands. The oxygen to silicon ratio of several SiO$_x$ thin layers deposited by thermal evaporation of silicon monoxide SiO and simultaneous oxidation are studied by FTIR spectroscopy in order to determine the stoichiometric degree x.

The infrared properties of the non-annealed and annealed samples at 1100 °C are presented in Fig. 2.6. Various silicon-oxygen related absorption bands can be identified in the wave number region from 700 to 1400 cm^{-1}. Due to the fact that the samples are produced under such conditions that they are totally hydrogen-free we can exclude all hydrogen related IR modes. The band around 810 cm^{-1} is attributed to Si−O textendash Si bond bending motion in SiO$_2$ [Tsu et al. 1989, Gucsik et al. 2004]. This band position increases when the sample composition approaches the pure stoichiometric silica (SiO$_2$) structure, while it is not detectable in the sample produced without excess oxygen exposure. The most intense feature in the spectra of Fig. 2.6 appears in the range of 1000-1100 cm^{-1}, which is ascribed to the Si−O−Si stretching vibrations [Lehmann et al. 1984]. The Si−O vibration frequency in thermally annealed samples shifts from 1034 cm^{-1} in the sample without excess of oxygen to higher frequencies at 1092 cm^{-1} in the sample of stoichiometric SiO$_2$ composition. The transversal-optical (TO) peak positions have been determined by the zero-transition of the

first derivative. The increase in wavenumber is due to the fact that the number of Si−Si bonds within the tetrahedral units decreases with the concomitant increase of Si−O bonds. The same fact can explain the creation and the frequency shift of the 810 cm^{-1} bending band. These peak positions can be used for a basic estimation of the stoichiometry of homogeneous SiO_x structures and as a measure for the phase transition from SiO_1 to higher x compositions SiO_x up to SiO_2.

In Fig. 2.7 we show the calibration of the stoichiometry degree x in SiO_x layers as a function of the Si−O−Si TO stretching mode frequency. We should mention that the position of the TO stretching mode as a function of the stoichiometric degree x is always expressed as a linear regressions-type formula, see e.g. [Tsu et al. 1989, Lehmann et al. 1984]. Different peak position determination methods could be the reason for the discrepancy between our data and those presented in the literature where mostly symmetric axis band positions have been used previously. Here we consider the zero transition of the first derivative to obtain the absolute peak position. Earlier a numerous equation in dependence on x was obtained [Lehmann et al. 1984]:

$$v_x = (48.8x + 976) \text{ cm}^{-1} \tag{2.5}$$

The estimated x values in a linear relation according to Lehmann [Lehmann et al. 1984] are shown as the dashed line in Fig. 2.7. Based on our IR data of the two well-calibrated and fixed SiO_1 and SiO_2 layers we had to slightly modify the Lehmann relation and have obtained the following approach for the growth of x in SiO_x from nearly $x>1$ up to stoichiometric SiO_2:

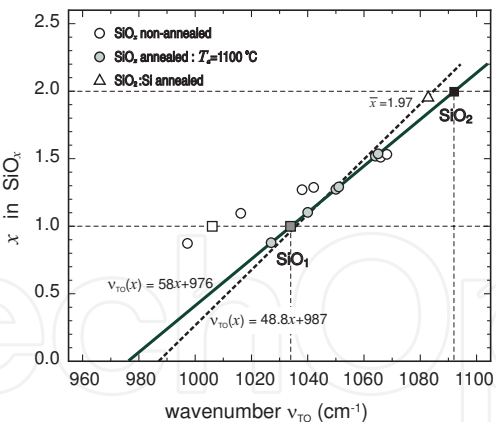$$v_x = (58x + 976) \text{ cm}^{-1} \tag{2.6}$$

Fig. 2.7 Calibration of stoichiometry degree x in SiO_x layers with the TO stretching mode of IR measurements; dashed line: according to [Lehmann et al. 1984]; solid line: given by the present SiO_1 and SiO_2 data of known stoichiometry, the wavenumbers of the annealed SiO_x samples were placed on this line; Δ SiO_2:Si ion-implanted sample from [Fitting et al. 2002b].

This relation is presented in Fig. 2.7 as a solid line for the thermally annealed samples, where $x=1$ and $x=2$ are given as fixed points and the other data were placed on this straight line between SiO_1 and SiO_2 in order to determine their x. Of course, the non-annealed samples will not fit to this straight line because their atomic network is still much more

Silicon Nanocluster in Silicon Dioxide: Cathodoluminescence,
Energy Dispersive X-Ray Analysis and Infrared Spectroscopy Studies

183

disordered than for the thermally annealed samples leading to higher TO mode softening, see Figs. 2.5 - 2.7. Additionally, a Si^+ ion-implanted sample SiO_2:Si with an Si excess of 4 at.% in the maximum of the implantation profile has been investigated previously, providing a mean stoichiometric degree over the full silica layer [Fitting et al. 2002b]. This value is close to $x=2$ but there is already a remarkable shift of $-\Delta v_{TO}=10$ cm^{-1} as can be seen in Fig. 2.7, supporting the sensitivity of the IR measurement.
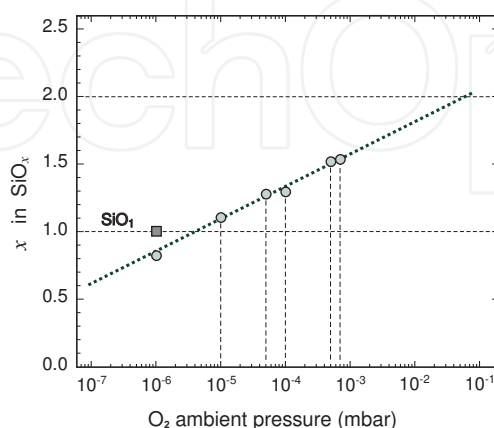
Fig. 2.8 Stoichiometry x of SiO_x layers as grown by thermal evaporation of SiO in oxygen ambient pressure, based on FTIR measurements after thermal annealing of the samples.

Then in Fig. 2.8 the x values obtained by FTIR are correlated with the ambient oxygen pressure during the evaporation of SiO_1. So the stoichiometric transition from SiO_1 to SiO_2 as a function of the ambient oxygen pressure can be estimated. An extrapolation shows that SiO_2 layers can be manufactured roughly at oxygen pressure nearly to 1×10^{-1} mbar.

2.6 CL of under-stoichiometric silica layers

In order to characterize the SiO_x layers by their optical luminescence features, cathodoluminescence (CL) studies of the SiO_x samples were carried out at both room temperature (RT) and liquid nitrogen temperature (LNT). see Fig. 2.9. This experiment was performed using samples that were thermally annealed at $T_a=600, 800, 1100, 1300$ °C besides the normal non-annealed samples, this way we could follow the structure change/growing under the influence of temperature treatment and the electron beam irradiation. Here we used also the experimental parameters as described before in the previous sections.

Samples with $x<1.3$ show almost no CL signals and samples with $x\approx1.3$ show quite weak and smoothed CL intensities even when they annealed at high temperatures or cold down to LNT. Thus, if the atomic ratio of silicon atoms is high compared with the ratio of oxygen, i.e. $x<1.3$, the samples do not exhibit any characteristic CL, indicating deficiency of Si−O bonds to form ordinary silica structures and any prominent silica defects.

Upon reaching $x>1.5$, the CL intensities grow considerably but almost only the yellow luminescence Y at 2.15 eV is detectable in the initial CL spectra (1 sec). After longer electron beam irradiation (30 min) the characteristic silica bands UV, B, and R appear too, as can be seen in Fig. 2.9.

Here the yellow Y luminescence band does not occur accidentally in hydrogen rich silica samples, there we have attributed a similar band to hydrogen molecules on interstitial sites in the silica network [Fitting et al. 2005a, Fitting et al. 2005b]. In Fig. 2.9 we see that the CL
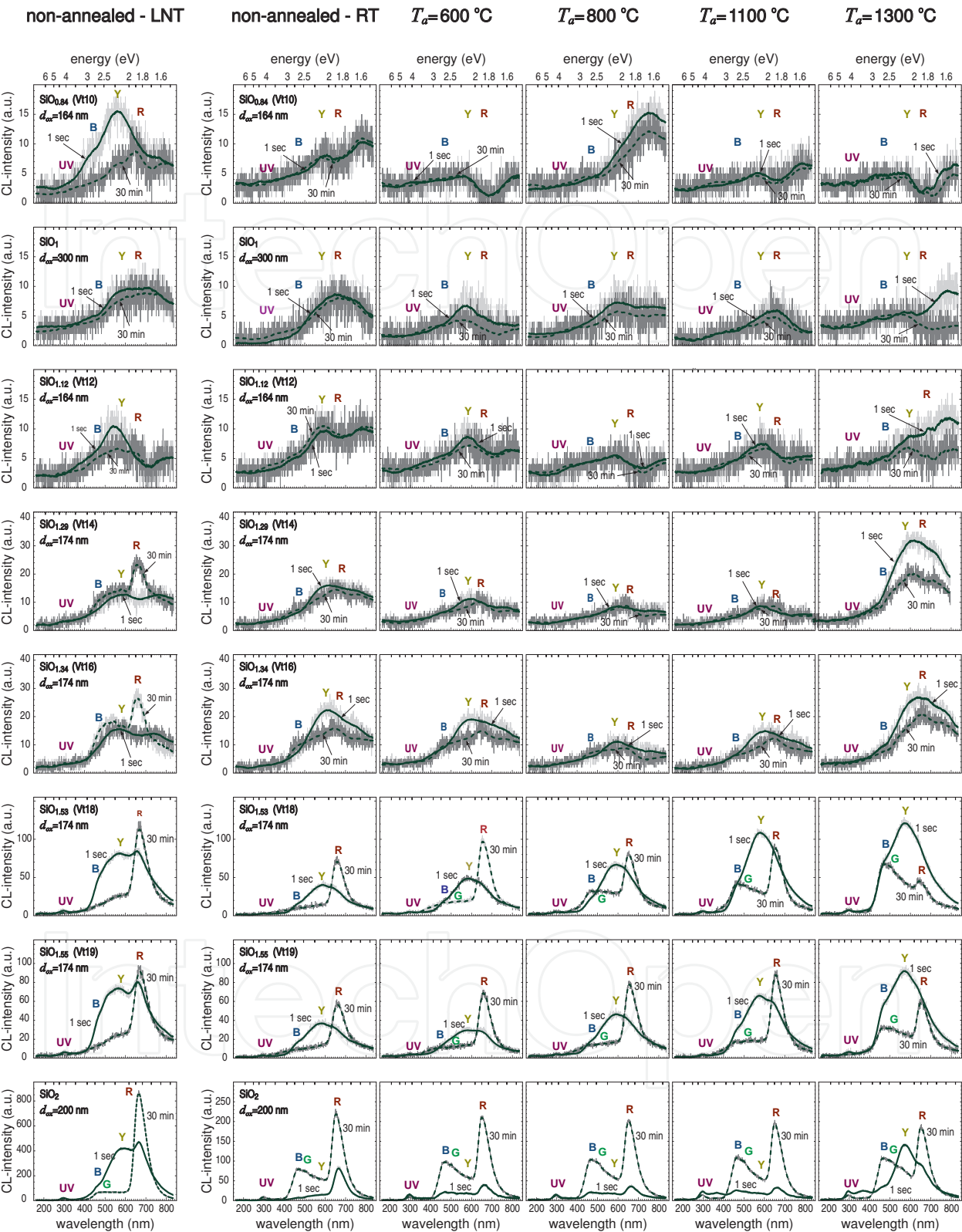
Fig. 2.9 CL spectra of SiO$_x$ layers with thickness d_{ox} grown on Si substrate with different ambient oxygen pressure and having been thermally annealed at different temperatures T_a. The initial and the saturated CL spectra are labeled by "1sec" and "30 min", respectively.
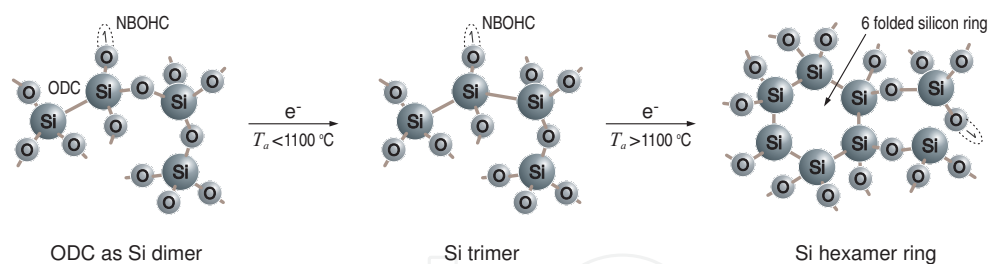
Fig. 2.10 Schematic presentation of the nonbridging oxygen hole center (NBOHC) and oxygen deficiency center (ODC) forming a Si dimer in the SiO_2 network (left) transformed by thermal annealing at temperatures T_a and/or electron beam irradiation to Si trimers (middle) and further on to elementary 6-fold silicon rings (Si hexamers) as a first step of Si nanocrystal formation (right).

spectra of dry and under-stoichiometric SiO_x layers (both are H-free), annealed up to relatively high temperatures in vacuum show a very intense yellow luminescent band at 2.15 eV. After annealing to temperatures T_a>1100 °C the Y luminescence is detectable too, even with higher intensity, which means it is increasing with T_a. We may conclude that the silicon atoms tend to re-arrange themselves in small clusters as chains or rings in the SiO_x network [Nicklaw et al. 2000], and that could be one of the most dominant origins for the Y luminescence in dry silica. In the absence of water there are strained bonds or defects of the form ≡Si−O⋯Si≡, where O⋯Si represents a strained (weak) Si−O bond that could be transformed into small membered silicon rings (3, 4-membered) [Ivanda et al. 2003] as well as to nonbridging oxygen hole centers (NBOHC) as an effect of high temperature treatment, as illustrated in Fig. 2.10.

A careful temporal observation of Fig. 2.10 makes it clearer that the cluster can be separated into core and surface components. The core is nucleation of silicon atoms (silicon bonded together) but on the surface both silicon and oxygen have dangling bonds, with the oxygen atom tending toward the surface. These fragments residing on the surface tend to be highly mobile [Schweigert et al. 2002], so we may state that the yellow luminescence is exciting from the surface of the silicon nanoclusters and not from the silicon core.

The red R (1.9 eV) emission is generally associated with the NBOHC and attributed to the recombination of electrons in the highly localized nonbridging oxygen band gap state with holes in the valence-band edge [Stevens Kalceff 1998]. On the other hand, tempering to T_a≈1300 °C leads to a further increase of the yellow band Y and to a strong reduction of the red band R. Probably, at these high temperatures oxygen is released from the SiO_x network diminishing the red luminescence but forming more oxygen deficient centers ODC and Si-rings.

In other words, more oxygen dangling bonds and oxygen deficient centers can be created due to high temperature exposure. Then silicon fragments or rings are produced in the silica network which seems to be the most probable candidates for the yellow Y luminescence center in silica.

2.7 EDX, CL and TEM investigation of Si cluster formation in modified silica

The formation of oxygen deficient centers (ODC) or even higher silicon aggregates by means of electron beam irradiation has been manifested already earlier [Fitting et al. 2002b, Trukhin et al. 1999, Fitting et al. 2005b, Stevens Kalceff 1998]. Even Auger electron spectroscopy (AES) has clearly evidenced that oxygen is dissociated from SiO_2 due to

electronic or thermal processes during electron beam excitation, see e.g. [Stevens Kalceff 1998, Cazaux 1986]. Thus the blue B and the red R luminescence bands grow under electron bombardment to a saturation after an irradiation dose of about 3 As/cm^2 [Fitting et al. 2002b], see the bottom row in Fig. 2.9.

In order to demonstrate the ODC increase during electron bombardment we have determined the stoichiometric degree x of SiO$_x$ by means of energy-dispersive X-ray analysis (EDX) during electron irradiation (E_o=10 keV, j_o=2 mA/cm^2) in initially stoichiometric silica layers SiO$_2$. The results are presented in Fig. 2.11. There we see a decrease of x with irradiation time, as expected, for room temperature (RT) faster than for liquid nitrogen temperature (LNT). The initial values with x>2.04 are somewhat higher than the expected ones x=2 of stoichiometric silica but we suppose an excess of oxygen on interstitial sites within the silica network remaining still from the oxidation process and the thermal diffusion of oxygen through SiO$_2$ towards the interface at the Si substrate. It is well known that over-stoichiometric silica with x>2 does not exist [Helm and Deal 1993], besides some peroxy bridges ≡Si−O−O−Si≡ or radicals as candidates or precursors for luminescent defects [Pacchioni et al. 2000], however, in very low concentration. This interstitial excess oxygen may form O$_2$ and O$^-_2$ molecules [Fitting et al. 2005c].
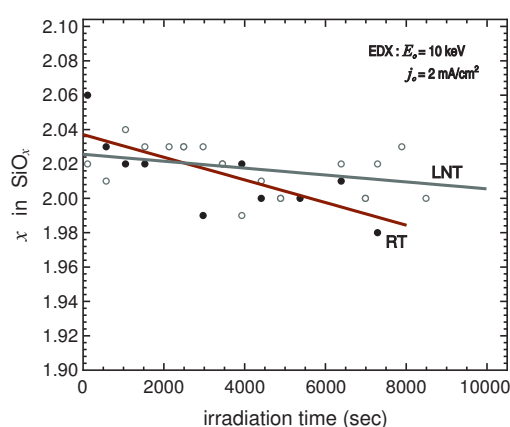

Fig. 2.11 EDX measurement of the oxygen to silicon ratio x in initially stoichiometric silica layers SiO$_2$ during electron beam irradiation at room temperature (RT) and liquid nitrogen temperature (LNT).
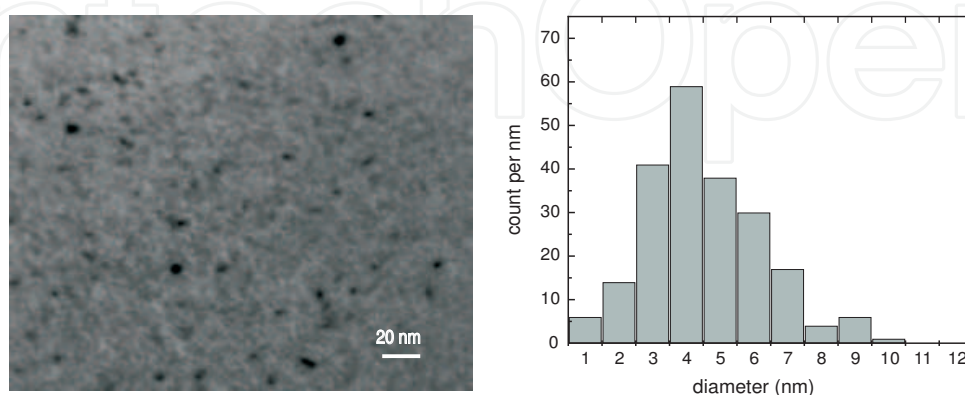

Fig. 2.12 TEM micrograph showing Si nanoclusters embedded in the silica matrix (left) and the related cluster size distribution (right) of a 250 nm SiO$_2$ layer having been irradiated for 30 min by an electron beam of 5 keV and 2.7 A/cm^2, [Salh et al. 2006].
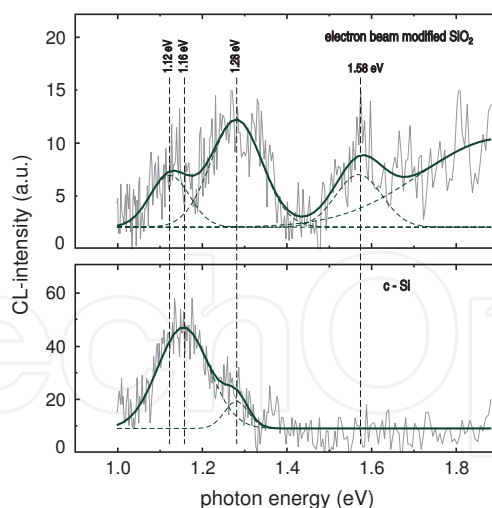
Fig. 2.13 CL spectra of electron beam modified SiO_2 showing in the near IR the fundamental transition of c-Si at hν=1.1 eV, of a-Si at 1.3 eV and a transition in Si nanocrystals (quantum dots) at 1.6 eV.

In order to demonstrate the oxygen dissociation and the formation of ODC, and finally, of Si clusters under electron bombardment we have carried out an additional experiment under high dose electron irradiation. Therefore thin 250 nm-thick silica films have been prepared by wet thermal oxidation on silicon wafers. Afterwards the silicon substrate had been removed by mechanical milling and 3 keV Ar+ ion etching. In this way self-supporting 250 nm thin silica films had been prepared for imaging in a transmission electron microscope (TEM). More details of preparation are given in [Kolesnikova et al. 2005].

These films were modified by heavy electron beam irradiation: beam energy 5 keV, current 20 nA over an area of 3/4 µm² yielding a high current density of 2.7 A/cm². Thus we may assume electronic as well as thermal dissociation [Kolesnikova et al. 2005] of oxygen from the thin SiO_2 layers and more and more the appearance of under-stoichiometric SiO_x. This SiO_x will undergo a phase separation as described by eq.(2.4). After 30 minutes of electron beam irradiation we observe Si cluster formation as presented in Fig. 2.12. The Si clusters embedded in the silica appear as dark spots. Their size distribution is shown in the right part of Fig. 2.12. There we see a most probable cluster diameter of 4 nm and a maximum diameter of 10 nm. As it has already been shown in the context of formation of Ge nanocrystallites in Ge-implanted silica, [Fitting et al. 2002b], such largely extended clusters will diminish the Si-related luminescence. The right size for elementary small luminescent clusters should be searched in intermediate regions, i.e. according to Fig. 2.10 between Si dimers (ODC) and hexamer rings.

Fig. 2.13 shows the CL spectra of pure crystalline Si and the spectra of Si nanoclusters embedded in the host silica. Luminescence bands are observed at around 1.1 eV and 1.3 eV assigned to crystalline and amorphous silicon phases, respectively. Another band at 1.6 eV is also to be seen after heavy electron beam bombardment in the SiO_2 structure. In spite of extensive experimental and theoretical work during the last years, the light-emitting mechanism which explains emission at 1.6 eV has not been fully understood yet. It is believed that the oxygen-related light-emitting centers are positioned at the interface between the Si nanoclusters and the host oxide [Prokes et al. 1998]. A broad CL emission band is characteristic of Si nanoclusters. Although the spectra vary considerably in intensity after longer irradiation, the peak position does not shift significantly, implying a similar

mean size for the nanocrystals. No unique relation between the CL or PL emission energies and Si nanocluster sizes has been reported in the literature making the quantitative comparison of the results difficult [Wilkinson and Elliman 2004]. Other authors estimated that 5 nm Si nanoclusters emit at 1.6 eV, while 3 nm Si nanoclusters give PL at 2 eV [Ledoux et al. 2002]. On the contrary it was reported that 4 nm Si nanoclusters emit at 1.3 eV and the 1.6 eV PL correspond to very small sizes of about 1 nm [Iacona et al. 2000].
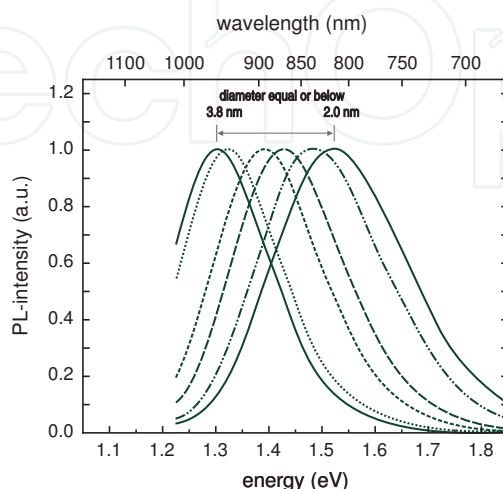

Fig. 2.14 Normalized photoluminescence spectra showing a blue shift correlated with the Si nanocrystal size, [Zacharias et al. 2002].
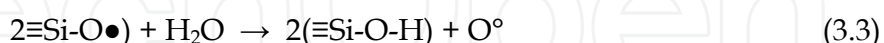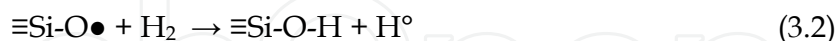
Recently Si nanocrystals have been fabricated by thermal treatment of SiO-SiO$_2$ nanolattices, in a way which makes it possible to control not only the size but also the density and the arrangements of the nanocrystals independently of the stoichiometry [Zacharias et al. 2002, Yi et al. 2003, Torchynska 2006]. In this method a strong photoluminescence (PL) and a size dependent shift of the PL position are shown as a proof of size control. A strong blue shift from 960 nm (1.3 ev) to 810 nm (1.5 eV) with decreasing nanocrystal size was observed with respective cluster sizes 3.8 nm and 2 nm, respectively, see Fig. 2.14.

3. Hydrogen implanted SiO$_2$

Direct hydrogen implantation or exposure of SiO$_2$ to water vapor results in the appearance of various OH bands, for example water molecules are known to form silanol (Si−O−H) groups in the oxide [Bakos et al. 2004b], but the relative concentration of silanol to interstitial water depends on the way the oxide was manufactured and subsequently treated, raising questions about the most stable form of water in the oxide and the role of hydrogen in this reaction. Hydrogen plays an essential role in the thermal oxidation process, either through the interaction with point defects or as interstitial atoms in the SiO$_2$ network. Hydrogen can be considered as an important accidental impurity or an intentional additive in all forms of silicon dioxide which can passivate dangling bonds and produce high-quality interfaces [Rashkeev et al. 2001]. Besides, it can reduce electrical activity of point and extended defects by inducing grain boundaries and it saturates oxygen dangling bonds (NBOHC ≡Si−O●) or the threefold-coordinated SiO$_2$ defect ($E´$-center ≡Si●), through the chemical reactions:

$$\equiv\text{Si−O● (or ≡Si●) +H}^\text{o} \rightarrow \equiv\text{Si−O−H (or Si−H)} \qquad (3.1)$$

where " $\equiv$ " denotes the three bonds and " $\bullet$ " represents the unpaired electron. Atomic hydrogen (H°) is unstable (mobile) above 130 K [Cannas et al. 2003b]. A variety of evidence strongly indicates that the dominant anneal mechanism for this atomic hydrogen is dimerization, (H°+H°→H₂). Hydrogen can also enhance the diffusivity of impurities or other interstitial atoms such as oxygen by forming water molecules. Water molecules are known to form silanol $\equiv$Si−O−H) groups even at room temperature:

$$\equiv\text{Si-O}\bullet + \text{H}_2 \rightarrow \equiv\text{Si-O-H} + \text{H}° \tag{3.2}$$

$$2\equiv\text{Si-O}\bullet) + \text{H}_2\text{O} \rightarrow 2(\equiv\text{Si-O-H}) + \text{O}° \tag{3.3}$$

Despite the wide interest in the behavior of H, paired H configurations (H₂) and H₂O in SiO₂, the understanding of the atomic scale processes remains limited and the microscopic identities of these electrically inactive H sites are the subject of intense debate. It is believed that the effectiveness of many defect generation and transformation processes depend critically upon sites where H can be trapped and released. We dedicate this section to presenting our results with hydrogen implanted SiO₂ layers.

3.1 CL of hydrogen implanted silica (SiO₂:H⁺)

Besides the main luminescence peaks: red R, blue B, and UV an amplification of the yellow luminescence Y at the region between 560 nm (2.2 eV) and 580 nm (2.1 eV) has been recorded due to direct hydrogen implantation especially at RT, see Fig. 3.1. In both cases, LNT and RT, the hydrogen implantation diminishes the red luminescence. Other authors [Morimoto et al. 1996] have used nearly the same implantation parameters (dose and implantation energy) as used in this study, and they reported the PL emission band at around 2.2 eV without a detection of the 1.9 eV band. Similar results are also obtained with He⁺ implantation [Morimoto et al. 1996]. As we present in hydrogen-implanted layers, Fig. 3.1, a yellow luminescence Y at λ≈575 nm (2.1 eV) is dominating the spectra and only a weak shoulder of the red luminescence appears. Here a high concentration of saturated bonds $\equiv$Si−O−H or $\equiv$Si−H) are expected, therefore the right hand side of eq. (3.1) is fulfilled where the NBOHC ($\equiv$Si−O$\bullet$) and $E´$-center ($\equiv$Si$\bullet$) are initially saturated by the excess hydrogen atoms. The $\equiv$Si−O−H bond is a good candidate to form NBOHC at room temperature in hydrogen rich silica. The NBOHC is possibly produced by breaking the H bonds at high annealing temperatures (T_a>1000°C) or under electron irradiation [Kuzuu and Horikoshi 2005]. Direct hydrogen implantation or H₂O molecule formation on the surface or in the silica network are believed to be the main reasonable source of the Y luminescence [Fitting et al. 2005b]; that means there are two aspects for the origin of this band.

3.2 Hydride ($\equiv$Si−H) and hydroxyl ($\equiv$Si−H−O) in SiO₂:H⁺

Hydrogen is a ubiquitous impurity in SiO₂, therefore some authors consider it an intrinsic defect. It is well known that hydrogen is present in all forms of silica. The wet oxide is proposed to contain around 10^{19} cm⁻³ OH groups (in the form of silanol or interstitial water molecules), while the typical OH concentration in dry oxides is only 10^{16} cm⁻³.

Interstitial hydrogen does not form covalent bonds with the network, and the hydrogen molecule does not react with the defect-free silica lattice [Blöchl 2000]. It has no states in the band gap of silica. Thus it may be difficult to activate the hydrogen molecule with UV light in the absence of other defects. This result indicates that hydrogen molecules need to
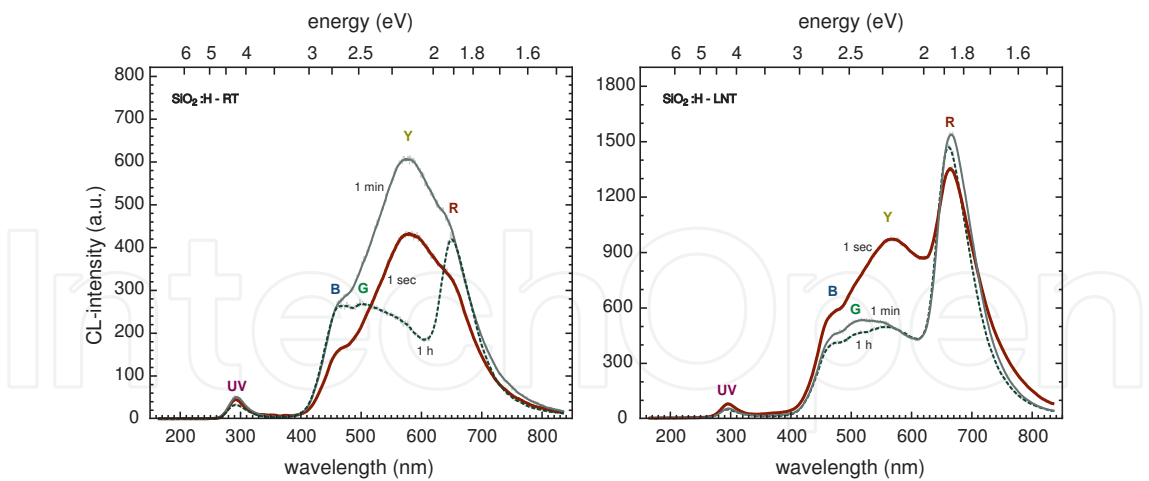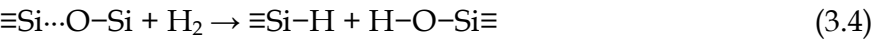
Fig. 3.1 Initial (1sec) and saturated (5h) and dose-dependent CL spectra of H⁺ implanted SiO₂ layers recorded at room temperature (RT) and liquid nitrogen temperature (LNT).

interact with defects in silica before they can be activated. That means interstitial H_2 molecules could react at least with broken or strained silicon bonds, as

$$\equiv Si \cdots O - Si + H_2 \rightarrow \equiv Si - H + H - O - Si \equiv \qquad (3.4)$$

or

$$D + H_2 \rightarrow \equiv Si - H + H - O - Si \equiv \qquad (3.5)$$

where D is an unspecified defect site. As we see, the product of the majority of the chemical interactions proposed so far is saturated defects which can be a source (precursors) for radiation induced defects later. In addition, hydrogen processing of the glass has been found to greatly improve the radiation resistance because it is suspected to reduce the number of precursors of radiation-induced defects [Brichard 2003]. It has been believed that OH bonds make the silica system softer and better able to resist the creation of many kinds of defects [Kuzuua and Horikoshi 2005].
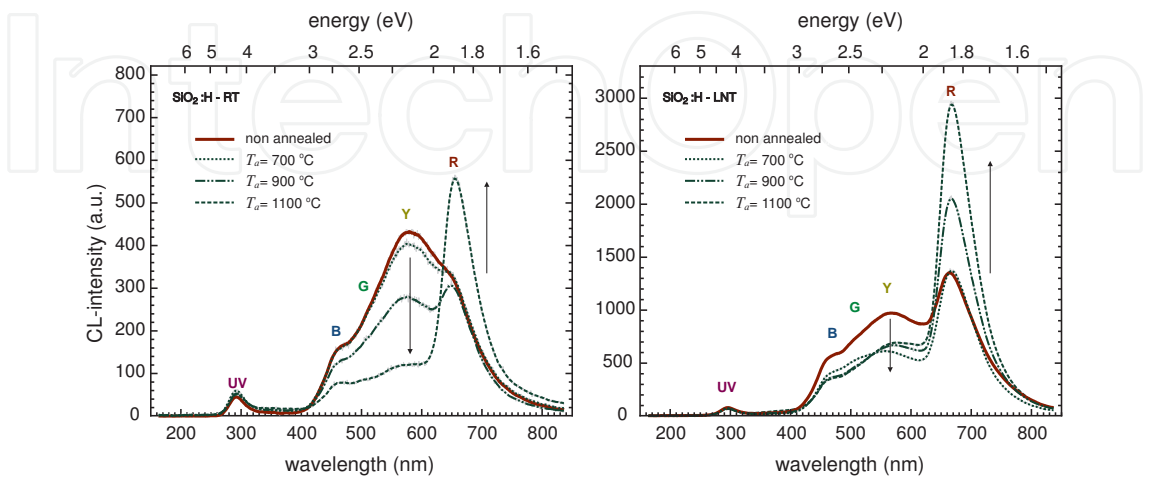

Fig. 3.2 Initial (1sec) CL spectra of H⁺ implanted SiO₂ layer at different annealing temperatures, 700≤T_a≤1100 °C, recorded at RT and LNT.

With additional hydrogen implantation we expect higher concentrations of both hydride (≡Si−H) and hydroxyl (≡Si−O−H) in the whole network which we consider as a first suspect for the dominant yellow luminescence in Fig. 3.1. If this hypothesis is correct, the yellow luminescence should possibly diminish by eliminating hydrogen from the system. Releasing hydrogen atoms even from amorphous material is previously reported by thermal treatment [Pan and Biswas 2004]. The samples have been thermally annealed up to relatively high temperature (T_a) so that we can state that we were able to break the hydrogen bonds and let an amount of hydrogen out. Fig. 3.2 shows a comparison between the non-annealed and those thermally annealed. We found a slight change in the intensity of the yellow luminescence at T_a=700 °C at both RT and LNT, which means that T_a=700 °C is not enough yet to make a significant change in ≡Si−H and ≡Si−O−H concentration. But by increasing the thermal annealing temperature to 900 and 1100 °C, we found a considerable change in the CL spectra. We see diminishing of the yellow luminescence and growing of the red luminescence R, leading us to the conclusion that T_a>900 °C can release hydrogen from both hydride and hydroxyl. The effective diffusion coefficient of hydrogen and the rate of ≡Si−O−H and ≡Si−H in hydrogen rich silica glass have been measured using Infrared spectroscopy [Lou et al. 2003]. It is found that the concentration of both ≡Si−O−H and ≡Si−H decreases due to sample thermal treatment, see Fig. 3.3. The decrease in hydroxyl quantity is very slow at 750 °C compared with other higher temperatures (1000, 1250 and 1500 °C). More and faster elimination of hydroxyl is achieved by increasing the temperature. A similar change in hydride quantity is also shown in Fig. 3.3. Our samples have been annealed for 3600 sec (the red vertical dashed line in Fig. 3.3) in vacuum, up to this period of time and T_a=1100 °C we can estimate that around 80% of hydride and hydroxyl have been eliminated from the SiO$_2$:H. In Fig. 3.4 (top), we signify the dose behavior of the yellow Y and the red R luminescence. The yellow band intensity shows higher initial level in the non annealed samples, it decreases by increasing T_a, but it passes a maximum at around 100 sec of electron beam irradiation. This means that other precursors for the yellow luminescence are produced. We consider short-term-living water molecule formation in the network to be one of these precursors. When H$_2$O molecules dissociate under the electron beam irradiation the yellow band starts to decrease.
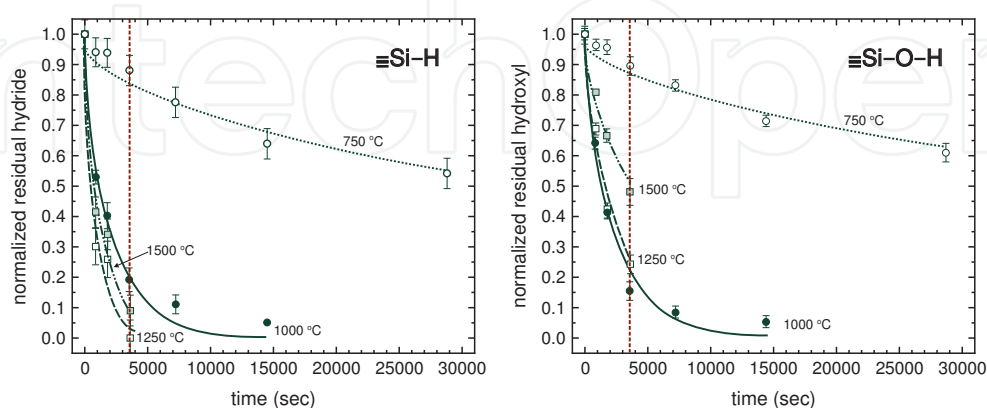

Fig. 3.3 Normalized residual quantities of hydride (≡Si−H) and hydroxyl (≡Si−O−H) as a function of heat treatment time in air. Open circle: 750 °C, filled circle: 1000 °C, open square: 1250 °C, filled square: 1500 °C, [Lou et al. 2003].

Contrary to the yellow luminescence, the red luminescence has much lower intensity in non-annealed samples and rises with increasing annealing temperature T_a until it shows the same dose behavior as the non-implanted wet a-SiO$_2$ layers as articulated in the previous section. We observe the same CL spectra and dose behavior of the red R luminescence in SiO$_2$:H as well as wet oxide SiO$_2$ samples at T_a=1100 °C, see Fig. 3.4 (bottom). Finally we can confirm the following production mode, eq. (3.6), of the non-bridging oxygen hole centers (NBOHC, ≡Si−O●), the source of the red R luminescence in wet oxide SiO$_2$, where hydrogen and hydroxyl are present.

$$\equiv Si-O-H \rightarrow \equiv Si-O\bullet + H^o \qquad (3.6)$$
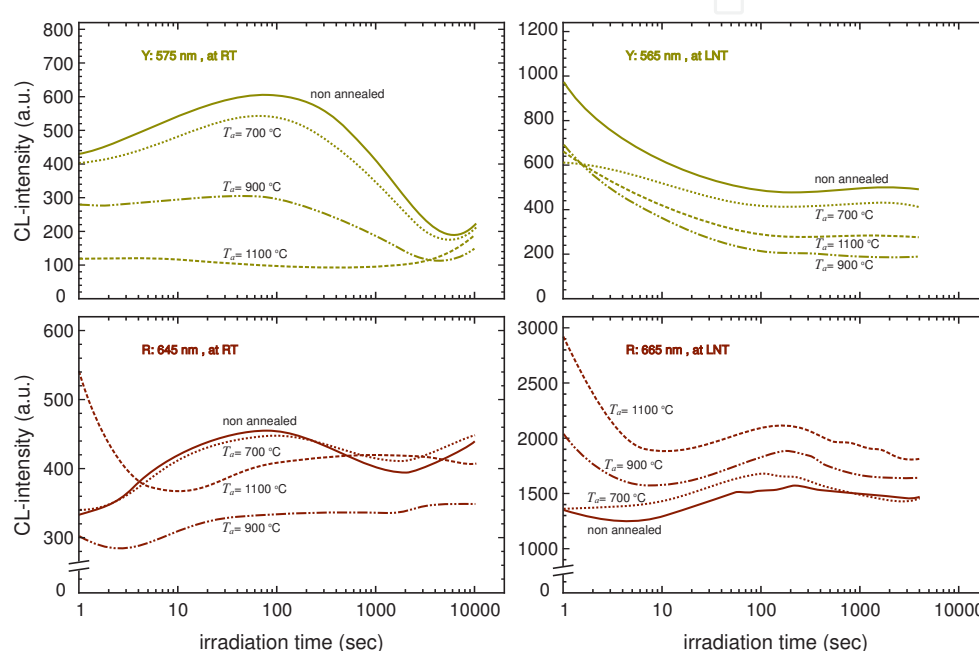

Fig. 3.4 The dose-dependent of the yellow band Y (top) and the red band R (bottom) in SiO$_2$:H at different annealing temperatures recorded at RT and LNT.

3.3 H$_2$O molecules and the yellow luminescence

The interaction of water molecules especially with the surfaces of amorphous silica is of great technological interest [Legrand 1998], and thus numerous studies have been devoted to this issue focusing especially on IR spectroscopy. It is suggested that the possible existence of small-membered (i.e. having a small number of members) Si−O rings on SiO$_2$ surfaces are expected to be the reactive centers for the interaction with water and other molecules [Mischler et al. 2005]. Additionally it is well known that water may dissociate on SiO$_2$ surfaces resulting in the formation of silanol (≡Si−O−H) groups. In particular it is frequently believed that the silanol groups are a result of the interaction of water molecules with small-membered rings [Mischler et al. 2005], see Fig. 3.5. Besides, some experimental results in the literature [Morimoto and Nozawa 1999] suggest that the photon irradiation of isolated ≡Si−O−H can lead to the formation of some hydrogen bonds between the hydroxyls and the H bonded ≡Si−O−H, which is decreased by heating to form once again isolated ≡Si−O−H and some H may be released.
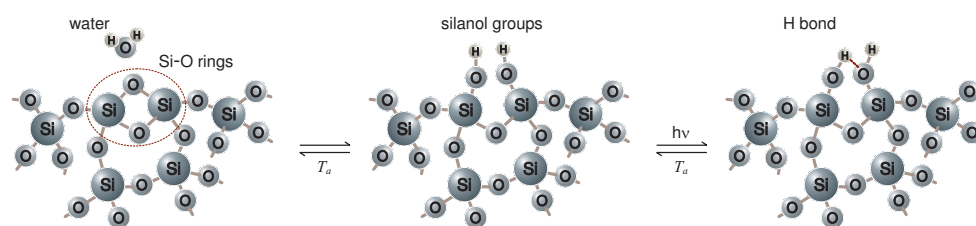
Fig. 3.5 The speculated equilibria showing the interaction of H_2O molecules with surface SiO_2 rings followed by a photochemical reaction of the $\equiv Si-O-H$ to the hydrogen bond. The dotted red line indicates the H bonding between H and O atoms, [modified after Mischler et al. 2005, Morimoto and Nozawa 1999].

Based on IR absorption spectra described by [Rinnert and Vergant 2003], the adsorption of water is favored by silicon dangling bonds (E'-center: $\equiv Si\bullet$) to form silanol groups not only on the surface but also in the silica network. The reaction between water molecules and the SiO_2 is supported too by the same authors, leading to the formation of two $\equiv Si-O-H$.

With some complexities we were able to produce a thin layer of ice on the surface of pure wet SiO_2 layer, whose CL behavior have presented in Fig. 3.6. Here we could measure the CL spectra of ice together with the typical CL spectra of SiO_2, see Fig. 3.6. Very intense yellow Y luminescence has been detected, even higher than the red R luminescence of SiO_2. An additional sharper band in the UV range ($\lambda \approx 370$ nm) is also clearly seen. The width of this band is much smaller than the conventional a-SiO_2 band widths indicating a crystalline structured H_2O. The whole spectral shape presented in Fig. 3.6 is loses its outlined profile in quite short time. We see that it is no longer possible to detect a luminescence band after some thirty seconds, especially the sharp band at 370 nm is totally disappearing.

A photoluminescence band at 3.7 eV (≈ 340 nm) has been reported in water-treated sol-gel synthesized porous silica. The authors have correlated this PL emission band indirectly to isolated silanols especially in the surface region [Yao et al. 2001], but others favored more the interacting OH-related centers [Anedda et al. 2003b].
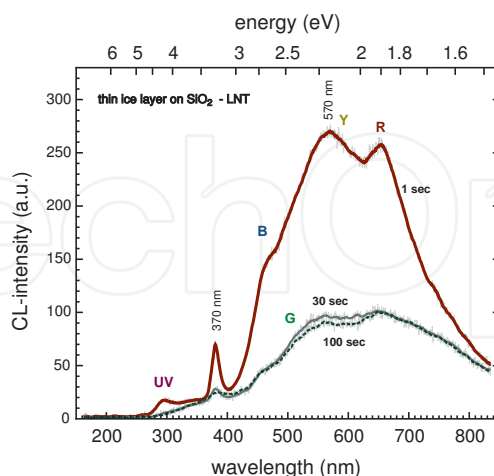

Fig. 3.6 CL spectra of a thin ice layer (H_2O) on SiO_2.

To determine whether the additional features presented in Fig. 3.6 belong to water molecules on the surface or not, we performed the same experiment where a thicker ice layer was produced on a metallic surface this time. To avoid any other influences coming from the substrate material, the metallic substrate was examined first; it gave absolutely no

CL signals in our sensitive detection region. The possibility of ice bilayers on metallic surfaces has been reported previously [Ogasawara et al. 2002]. It was found that half of the water molecules bind directly to the surface metal atoms and the other half are displaced toward the vacuum in the H-up configuration.

Ice layers on a metallic substrate show similar initial spectra with both 570 and 370 nm emitted CL bands; they start with very stable intensities but the intensities fall down rapidly due to the heat produced by the electron beam where the ice layer begins to melt then, see Fig. 3.7.
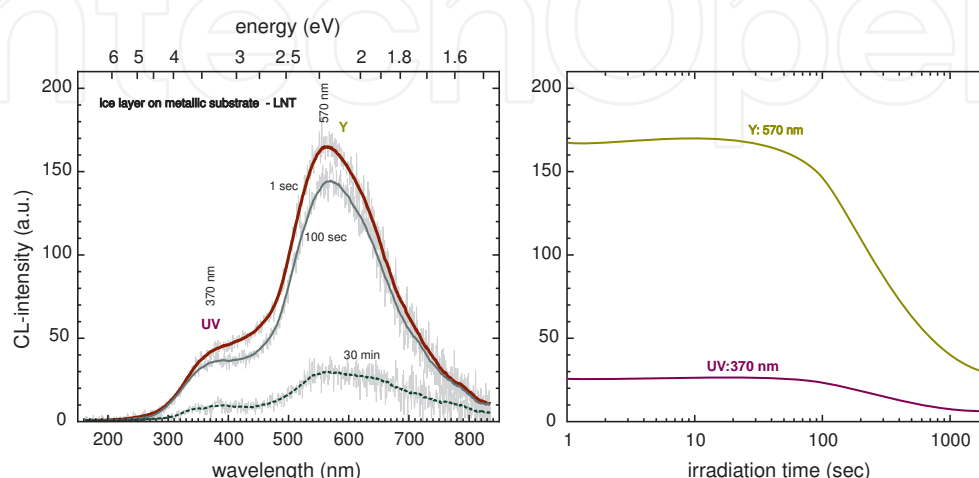

Fig. 3.7 CL spectra of thin ice (H$_2$O) layer on a metallic substrate (left), the dose behavior of the individual luminescence bands (right).

Thus we state that both the fast decreasing yellow Y band at 570 nm, 2.15 eV (formerly called green-yellow band G) as well as the long-term irradiation Y band is the same electronic state and all attributed to water. In the first case condensed water and ice sublimate at LNT from the surface whereas the longer irradiation Y band is due to water molecules formed in the SiO$_2$ network by radiolytic processes.

3.4 Hdrogen association in luminescence defects

Extrapolating from the facts presented up to now we can formalize a model for the different luminescence properties of the radiation induced defects in a-SiO$_2$, presented in Fig. 3.8. We assume that strained bonds ≡Si−O··Si≡ in dry oxide and the hydroxyl species (≡Si−O−H) in wet oxide are the prevailing main precursors of the red R luminescence associated with non-bridging oxygen hole center (NBOHC: ≡Si−O●).

During electron beam irradiation both precursors are transformed to NBOHC. We see that the NBOHC centers produced in dry oxide increase up to a certain concentration obtained by an equilibrium of center generation and electron beam induced dissociation to the E'-center (≡Si●) and mobile atomic oxygen O$_{mob}$. The production and the role of mobile oxygen have already been stressed by [Skuja et al. 2002 and Fitting et al 2002b]. There, a model and respective rate equations are given for the temperature and dose dependence of both the red R and the blue B bands. The re-association of mobile oxygen to the E'-centers and re-creation of the NBOHC will increase the role of mobile oxygen and hydrogen. Experiments had suggested that the ≡Si−O−H is resisting bond breakage effectively at relatively short irradiation time. Bond breakage might saturate only at sufficiently long irradiation time [Kuzuu and Horikoshi 2005]. Different properties are shown by the wet oxide in Fig.3.8.

Here the hydrogen is dissociated from the silanol group of the non-bridging oxygen bond, eq. (3.6). But then the red luminescence of the NBOHC is destroyed by further electron beam dissociation as in dry oxide too. The dissociated mobile hydrogen H_{mob} may react with the mobile oxygen O_{mob} to form molecules H_2, O_2, and H_2O on interstitial sites. These reactions have been recently described [Bakos et al. 2004a]. There the authors underlined that water and oxygen molecules are participating in various defect formation processes in thermally grown SiO_2 films as well as in synthetic silica glasses. Formation energies and energy barriers are obtained by first-principles calculations and compared for different reactions. A part of the H atoms on the right-hand side of eq. (3.6) must form H_2 molecules through the diffusion of H atoms in the silica network. In addition to H_2 molecules produced by this mechanism, interstitial H_2 molecules are expected to exist in the sample. These H_2 molecules and interstitial H_2 molecules could react with broken or strained bonds and form $\equiv Si-H$ and $\equiv Si-O-H$ pair as in eq. (3.4).

The $\equiv Si-H$ structure on the right hand side of eq. (3.4) can be a precursor of the $E´$-center through the process expressed in the reverse of eq. (3.1). The amount of H_2 molecules created by the irradiation must increase with increasing OH content. In addition to the creation of hydrogen molecules from the $\equiv Si-O-H$ species, interstitial H_2 molecules exist especially in the wet samples. Therefore, an excess amount of $E´$-centers, relative to that of NBOHC, is induced as shown in Fig. 3.8.

Water molecules may cluster in the bigger voids of the oxide, i.e., form hydrogen-bonded complexes with each other and the silica network's O atoms [Bakos et al. 2004a]. In such cases two H_2O molecules may react with each other forming once more OH bonds. Thus, the red luminescence is stabilized at some fraction of the number of OH bonds. This model of the hydrogen effect is consistent with our previous model of center transformation based on the mobile oxygen generation and re-association [Fitting et al. 2002b], and extends it by the reactions of H, OH, and H_2O with the radicals in the silica atomic network as shown in Fig. 3.8. This model is supported by investigations of the yellow Y luminescence, where the yellow luminescence at the beginning of irradiation at LNT is associated with sublimating ice from the sample surface rather more probably than due to a self-trapped exciton (STE) luminescence as often emphasized [Trukhin 1994]. Moreover, the yellow Y luminescence after longer irradiation (2 As/cm²), especially in hydrogen implanted samples, could be associated with water molecules H_2O too, formed in radiolytic processes as demonstrated in Figs. 3.6 and 3.7.

4. Group IV elements implanted in SiO_2

Ion implantation into glasses results in network damage and in compositional changes, it modifies silica's physical properties such as density, refractive index, surface stress, hardness, and chemical durability. Compositional changes can also occur due, e.g., to radiation-enhanced diffusional losses of alkali ions, crystallization, phase separation, and H incursion. Many authors [Hosono et al. 1990, Morimoto et al 1996, Fitting et al. 2002b, Magruder et al. 2003] have implanted several kinds of ions in silica glass and found that ion implantation causes an increase in refractive index by 1%-6% owing to the compaction of surface region and to a chemical change in the structure of glass. It was deduced that this refractive index change is caused by the formation of Si\textendash Si homobonds, but not by the decrease in Si−O−Si bond angle which leads to compaction. In addition to the compaction, the chemical change in structure, and the formation of colloid particles, ion
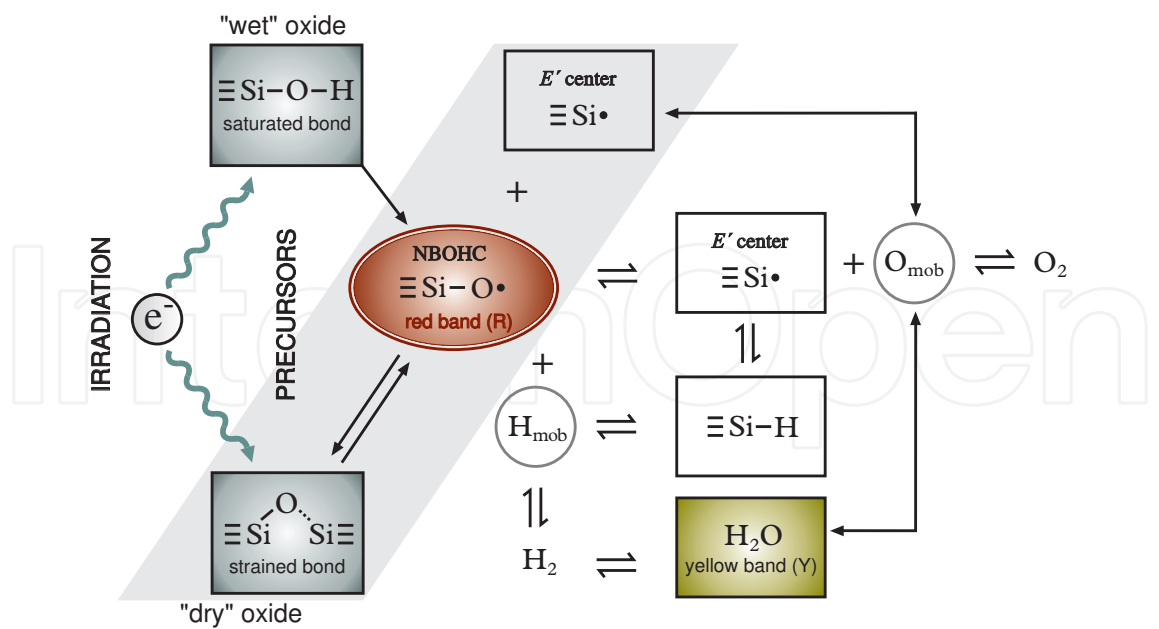
Fig. 3.8 Model of the red luminescent center (NBOHC) creation from different precursors in "wet" and "dry" oxide. The center destruction and recombination by radiolytic hydrogen and oxygen dissociation and re-association will lead to a dynamic equilibrium.

implantation in silica glass is always accompanied by the formation of defects, such as oxygen vacancy, E'-center, NBOHC, and peroxy radicals, resulting not only in changes to emission bands but also to the emission of new CL bands especially in the violet V or in the ultraviolet UV regions.

Before we start reviewing our results, it is appropriate to keep in mind that there are species which diffuse through the glass without modifying the structure of the matrix, and these are called non-interacting elements. There are both interstitial and substitutional non-interacting species. Species which modify the structure of the glass matrix are called interacting species [Minke and Jackson 2005]. Carbon (C), silicon (Si), Germanium (Ge), tin (Sn) and lead (Pb) are the dopants whose influence on silica's natural luminescence defects will be discussed in this section. They are examples of non-interacting substitutional species. Since these elements have similar bonding characteristics to silicon, they can replace silicon in the matrix of the glass, without significantly changing the network structure. Substitutional non-interacting elements diffuse much more slowly than interstitial elements. Ion implantation results allow deeper understanding of the relationship of the structure to dopand incorporations, which is important for the application of ion implantation wave guide formation in optoelectronic applications.

4.1 Silicon implantation SiO$_2$:Si$^+$

To get started with the investigation of the implanted samples, we prefer to recognize especially the surplus of atoms from the host material in this complex many body correlated system. We report in this section our observation of visible-light emission at room temperature from Si$^+$ implanted thermally grown SiO$_2$ layers on silicon substrates. Cathodoluminescence measurements were performed on silicon implanted samples using the same experimental parameters as used for the non implanted samples. As a result of comparison between the CL spectra of the pure and Si$^+$ implanted SiO$_2$, we see a significant

blue B luminescence emission (460 nm ; 2.7 eV) and an intense broad luminescent band in the yellow Y region with a peak beyond 580 nm (2.1 eV) are observed especially after annealing at high temperature (T_a=900 °C), see Fig. 4.1. The ultra violet UV (290 nm ; 4.3 eV) and the red R luminescence (650 nm ; 1.9 eV) are also present but with less influence due to silicon implantation. Two additional luminescence bands can be anticipated, one in the green G region at 490 nm (2.5 eV) and another in the red region at around 750 nm (1.65 eV). Higher initial intensities in the thermally annealed samples were registered but all luminescence were saturated to the same level as of the non annealed samples. The green (490 nm ; 2.5 eV), yellow (580 nm ; 2.1 eV) and the additional red (750 nm ; 1.65) emission bands are associated with the presence of silicon nanoclusters in the silica matrix.
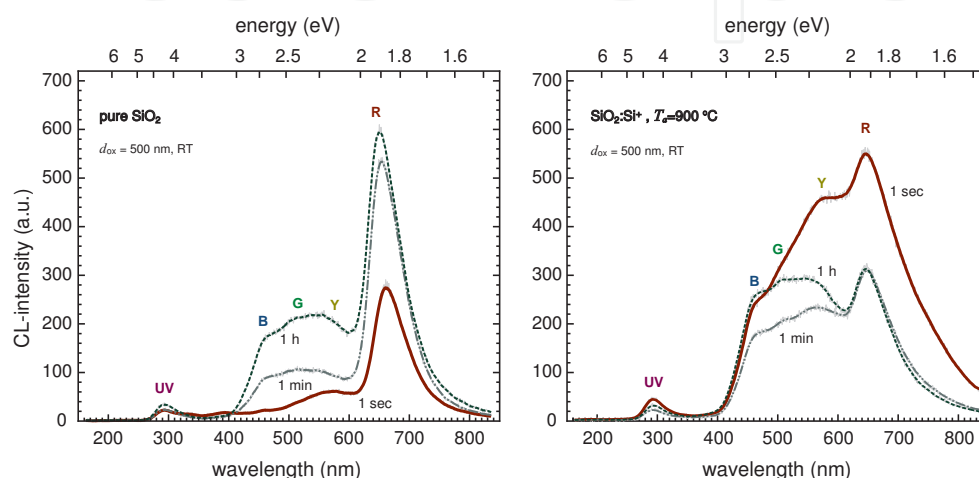

Fig. 4.1 CL spectra of pure and Si⁺ implanted SiO₂ layers at room temperature (RT). The initial spectra (red colored) is labeled by (1 sec) and the saturated by (1 h).

The presence of silicon nanoclusters (crystalline and amorphous) is confirmed by transmission electron microscopy (TEM) and by means of EDX measurements. Recently, some authors presented room-temperature photoluminescence data from silica layers implanted with Si⁺ ions of 160 keV energy excited using 292 nm excitation light from a 450 W xenon lamp [Mutti et al. 1995]. They showed the existence of a visible band peaked at 1.9 eV (620 nm) together with a broad band centered at lower energy 1.7 eV (730 nm) which was present only after annealing at 1100 °C. They ascribed the 1.9 eV band to $E´$ defects created by ion implantation in the silica matrix, while they attributed the 1.7 eV band to the presence of silicon nanocrystals.

4.2 Germanium implantation SiO₂:Ge⁺

Typical CL spectra of Ge⁺-implanted silica layers at room temperature (RT) are shown in Fig. 4.2. The main ultraviolet (UV) and violet (V) luminescence bands at 295 nm (4.2 eV) and 410 nm (3.1 eV) respectively, and a green band around 535 nm (2.3 eV) are seen predominantly on non-annealed samples even at low temperature. The well-known red band appears also in our detection range but not as dominant band as in the standard SiO₂ spectra. Previously we have demonstrated that the spectra of Ge-doped amorphous SiO₂ layers are a mixture of SiO₂ and tetragonal GeO₂. Whereas the red luminescence at 1.9 eV from the NBOHC of the SiO₂ matrix is conserved, the larger amplitude of the violet band at 3.1 eV seems to be overtaken from tetragonal GeO₂ modification indicating a

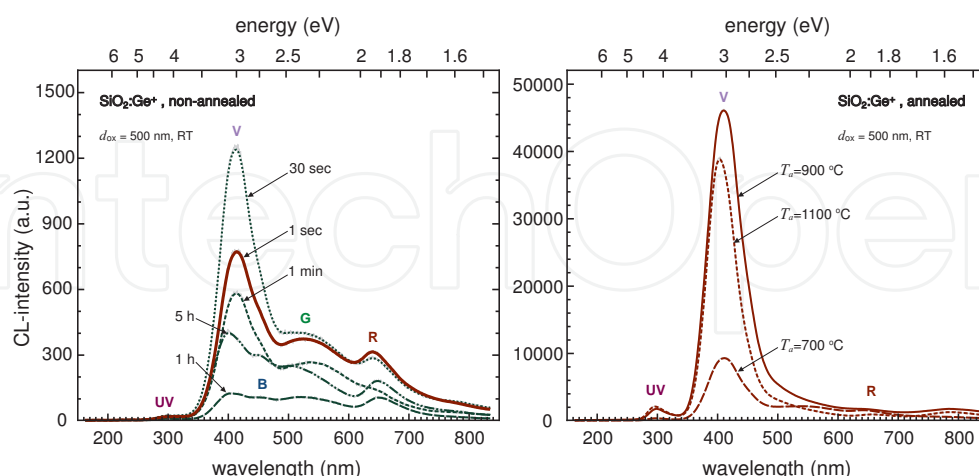strong defect luminescence at the Ge dopant centers in the rutile-like tetragonal coordination [Barfels 2001].

Fig. 4.2 CL-spectra of Ge+-implanted (500nm) SiO$_2$ layers (implantation dose D=5×10^{16} cm^{-2} recorded at RT on the left hand side, demonstrating the huge violet band (V) at λ≈410 nm: 3.1 eV. The thermal annealing of the samples was performed at three different annealing temperatures T_a=700, 900, 1100 °C, as shown on the right hand side.

The CL spectra of pure undoped a-SiO$_2$ and Ge+-doped are similar to the local intrinsic point defect centers associated with the fundamental silicon dioxide defect structure. The energy positions and widths of the red R and the UV CL emissions are the same for both specimen types within the limits of experimental uncertainty, unless the violet band (λ≈410 nm, 3.1 eV) is considered to be a well seen fingerprint of Ge related defects and covering the blue band (λ≈465 nm, 2.7 eV) of pure SiO$_2$. According to an earlier model [Skuja 1998], the violet luminescence corresponds to the so-called twofold coordinated germanium luminescence center (=Ge●●) which imperceptibly interacts with the host material atoms due to its poor correlation in the silica glass network. However, this band could be also associated with different phases of Ge, that is to Ge clusters as well nanocrystals located in the SiO$_2$ layer [Fitting et al. 2002b], which can remarkably grow in size with increasing post annealing temperature. In the absence of Ge impurities, the luminescent emission component observed between 3.1-3.3 eV in oxygen deficient silica has been attributed to the recombination of a hole trapped adjacent to a substitutional charge-compensated aluminum ion center [Stevens-Kalceff 1998].

Furthermore, Fig. 4.2 (right) shows the CL spectra of the Ge+-implanted sample annealed at 700, 900, 1100 °C for 1 hour in dry nitrogen. The large emission band at 3.1 eV due to the germanium implantation is observed and the intensity of this peak increases up to a factor of 10-50 with increasing annealing temperature (T_a), but it decreases rapidly with increasing irradiation time. The concurrent changes in the various bands of the emission spectra due to the Ge implantation are shown in Fig. 4.3.

With increasing annealing temperature up to T_a=900 °C the CL intensity strongly increases. Exceeding the annealing temperature up to 1100 °C, i.e. to the original oxidation temperature, the CL intensity is reduced again and the green luminescence intensity at 535 nm is terminated (totally annealed), contrary to the violet (V) luminescence band which still shows an enormous presence in the CL detection range. Also we see that NBOHC fades

Silicon Nanocluster in Silicon Dioxide: Cathodoluminescence,
Energy Dispersive X-Ray Analysis and Infrared Spectroscopy Studies

199

away with increasing annealing temperature (Fig. 4.3). That could be somehow a reason of activation of various interstitial atoms at high temperatures, where electron spin resonance (ESR) experiments have shown that the thermally activated diffusion of mobile interstitial species can result in the annealing of defects involved in luminescent processes [Griscom 1990b]. As we stated, the violet luminescence is related to different states or phases of Ge, namely to GeO_2 dissolved in the near SiO_2 surface region and to Ge nanocrystals [Rebohle et al. 2002a] located in the SiO_2 layers, see Fig. 4.4, which may be partially oxidized at their interface to the surrounding amorphous SiO_2 matrix. The nanoclusters size are growing with annealing temperature from 2-4 nm at T_a=900 °C to 5-10 nm at T_a=1100 °C as shown in Figs. 4.5 and 4.6.
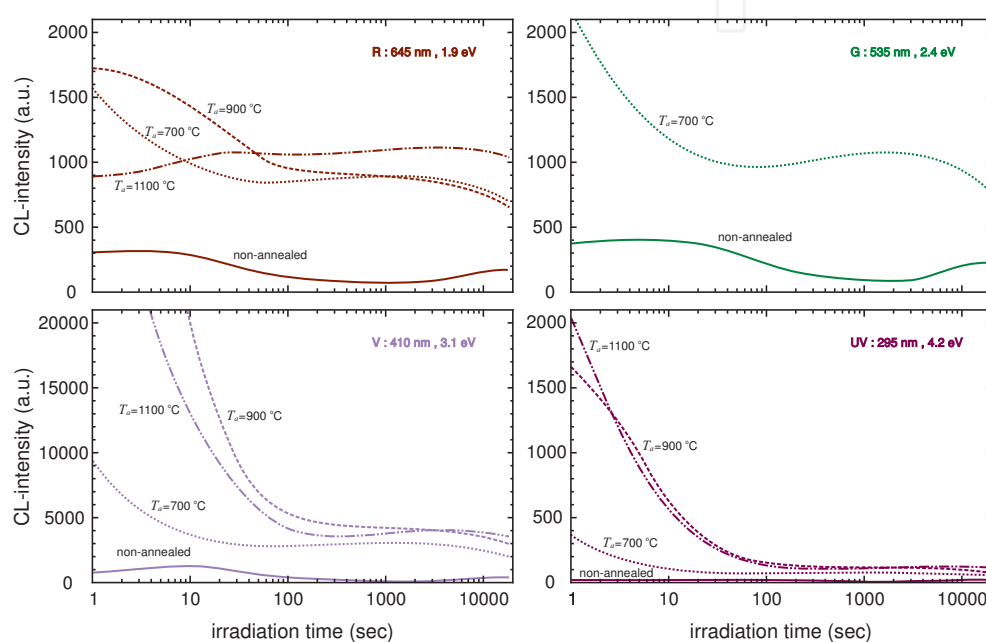

Fig. 4.3 CL bands red (R:1.9 eV), green (G:2.4 eV), violet (V:3.1 eV) and (UV:4.2 eV) from Ge⁺-implanted SiO_2 layers after different annealing temperatures T_a as a function of irradiation time; CL measured at RT.

High resolution TEM micrographs shown in Fig. 4.5 reveal a spherical shape of Ge nanocrystals in silica, in contrast to the shape of nanocrystals in other crystalline host material. This is apparently the result of the anisotropy of the amorphous silica matrix. Further experimental analysis of the orientation relationships between the nanocrystals and the crystalline matrix shows that there is no fixed relationship of orientation between the nanocrystals and the host [Xu et al. 2005]. A closer look at the highly resolved area is obtained (marked by light colored circles) in Fig. 4.6 where higher magnification was applied. The white circles enclose some of the nanocrystals visible under this magnification. The crystalline structure (lattice) pattern of germanium nanoparticles is clearly distinguishable from the amorphous host, in some areas similar even smaller crystal lattices overlap each other. The host matrix remains in amorphous phase surviving the implantation and thermal annealing.

The size distribution of the Ge nanocrystals was obtained through a laborious TEM effort of a micrograph of very thin cross-sectional TEM specimen, and then followed by manually measuring the size of the nanocrystals. The result is shown in Fig. 4.7. The dark bar
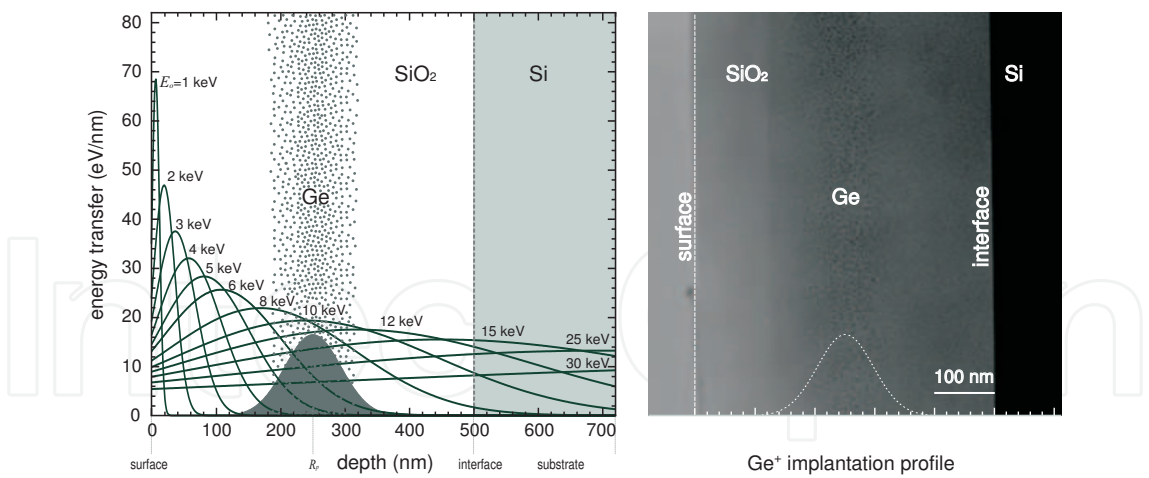
Fig. 4.4 Electron beam excitation densities in SiO$_2$ layers on Si substrate for different beam energies E_o allowing a CL depth profiling. Here we show the Ge$^+$ implanted SiO$_2$ in the mean projected range R_p=250 nm by an ion energy E_{Ge+}=350 keV shown by the shaded Gaussian shaped region. On the right hand side a scanning transmission electron microscope (STEM) image of the same sample showing the actual Ge cluster profile after thermal annealing.
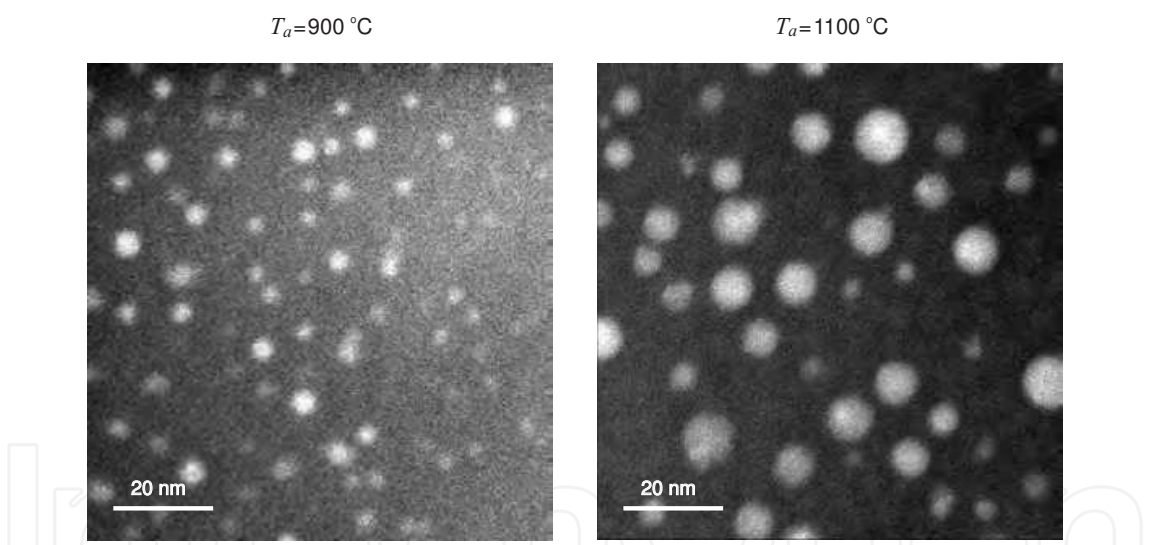

Fig. 4.5 Scanning transmission electron microscope (STEM) images of germanium implanted SiO$_2$ sample annealed at: T_a=900, 1100 °C, showing the actual size of the Ge clusters.

histogram shows the size distribution of Ge nanocrystals embedded in silica produced at T_a=1100 °C and the light bars are the size distribution of nanocrystals formed at T_a=900 °C. The Ge nanocrystals at higher temperatures are larger on average and have a wider size distribution than those formed at lower temperatures, as it was expected. The size distribution of the germanium particles in the silica system is near-Gaussian-shaped, corresponding to average diameters of 3 nm and 6 nm for T_a=900 and 1000 °C, respectively. The cluster density is also shown in Fig. 4.7, where the cluster concentrations are N$_c$=4.6×10^{17} and 2.6×10^{17} cm^{-3} for T_a=900 and 1100 °C, respectively. It is expected that thermally treating the samples is not the only reason for nanocluster formation but also

Silicon Nanocluster in Silicon Dioxide: Cathodoluminescence,
Energy Dispersive X-Ray Analysis and Infrared Spectroscopy Studies

201
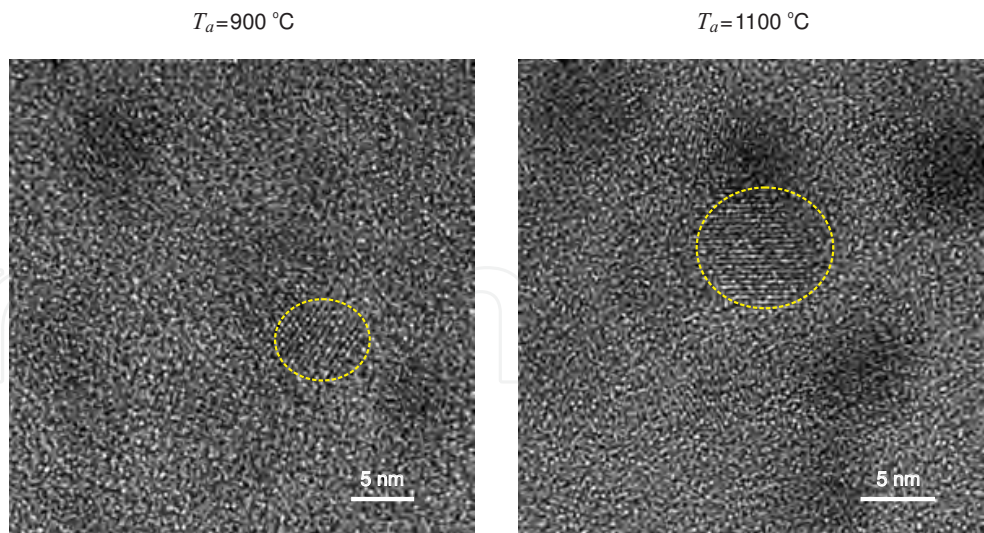
Fig. 4.6 HR-TEM micrograph of Ge-implanted SiO_2 layers after 1 h anneal at 900 , 1100 °C. Selective areas in the host matrix showing the growing of the crystalline Ge spots with increasing temperature.
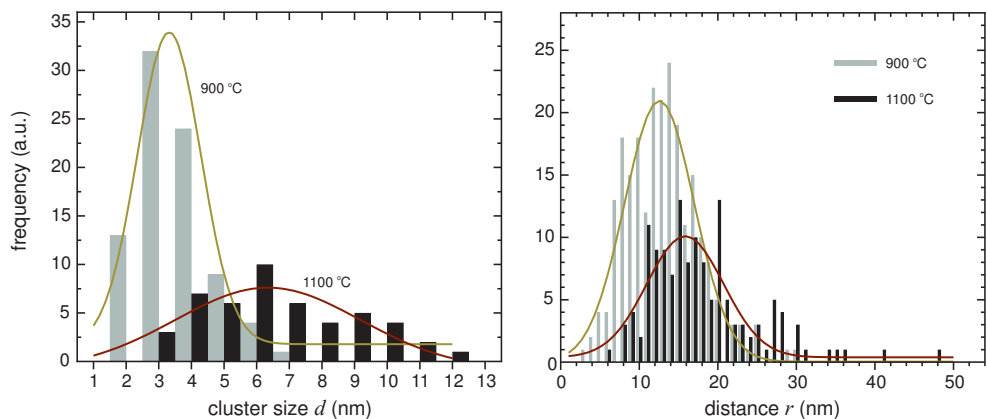

Fig. 4.7 Germanium cluster diameter and separation distance distributions: the correlated cluster concentrations are $N_c = 4.6 \times 10^{17}$ and 2.6×10^{17} cm^{-3} for $T_a = 900$ and 1100 °C, respectively.

heavy electron beam irradiation, where Ge atoms diffuse faster in the more damaged area caused by the irradiation. Large nanocrystals are thus formed, whereas in the area where Ge atoms are less mobile, smaller nanocrystals are formed.

Based on the assessments specified in this section , we are presenting a model in Fig. 4.8 of the annealing process forming Ge aggregates with an optimum size for a maximum luminescence at annealing temperatures near $T_a = 900$ °C. For higher annealing temperatures $T_a \geq 1100$ °C the cluster or crystal growth has continued, thus their luminescent surface or surroundings in their sum has been reduced, i.e. the overall luminescence efficiency decreases. Simultaneously the specific depth of luminescent Ge clusters, however now in a lesser amount, has shifted towards the surface, whereas at greater depths we find bigger Ge crystallites but much less effective in luminescence than the smaller clusters.
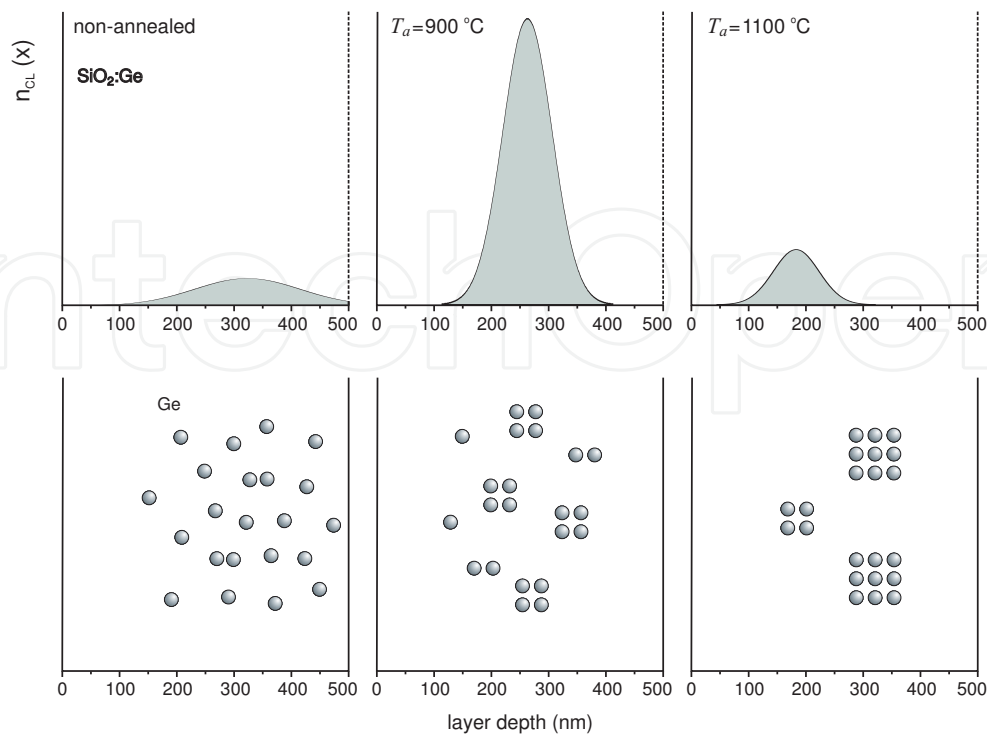
Fig. 4.8 Schematic presentation of the luminescent center depth profile as a function of post annealing temperature T_a (above) and the supposed depth distribution of Ge nanocrystals (below) with an optimum size for maximum luminescence (middle part).

4.3 Carbon implantation $SiO_2:C^+$

Carbon implantation, like other ion implantations, produces many different chemical reactions. It has been observed that the implanted carbon in silica can form carbon dioxide (CO_2) and carbon monoxide molecules (CO) [Perez-Rodriguez, et al. 2003]. It is intriguing that the CO and CO_2 formed in the silica matrix have a very different spectroscopic behavior from that of the gas phase molecules. These differences may reveal the unique physical statuses of the CO and CO_2 embedded in the matrix. C^+ implantation is usually combined with Si^+ implantations (Si rich SiO_2 layers), whereas in SiO_2 layers implanted only with C^+ ions, it has been evidenced early on that a severe drawback consists in the strong outdiffusion of the implanted carbon during the thermal process. This is caused by the formation of highly mobile CO species. Accordingly, these phenomena could be prevented by annealing under high-vacuum conditions. However, the most interesting approach to stabilize the implanted C profile is the previous existence of a high Si supersaturation, which enhances the interaction of both C and O atoms with the Si atoms, and prevents the formation of C−O bonds. In this respect, we discuss the CL spectra of C^+ implanted silica.

High dose sequential implantation of C^+ ions into the SiO_2 oxides followed by high-temperature annealing (T_a=900 °C) probably results in the mixture of violet-blue-green-yellow luminescence. The observed visible luminescence bands have been correlated with the implant and annealing conditions and with the microstructure of the processed films.
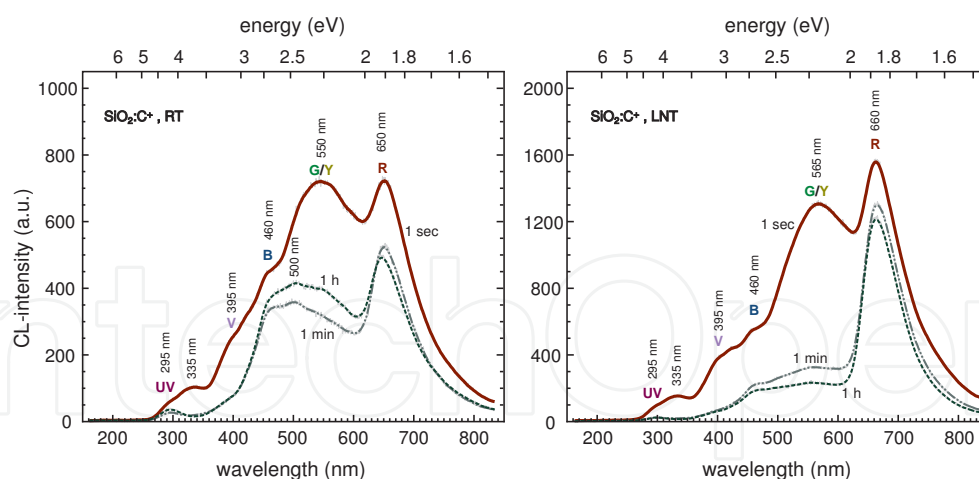
Silicon Nanocluster in Silicon Dioxide: Cathodoluminescence,
Energy Dispersive X-Ray Analysis and Infrared Spectroscopy Studies

203

Fig. 4.9 CL-spectra of C$^+$-implanted (500nm) SiO$_2$ layers (implantation dose D=5×10^{16} cm^{-2} recorded at RT and LNT. The sample was thermally annealed at T_a=900 °C.

Fig. 4.9 demonstrate the CL spectra of C$^+$ implanted SiO$_2$ layers at room temperature (RT) and liquid nitrogen temperature (LNT). A significant difference due to the measured temperature change has not been registered. In general, it is more similar to the CL spectra of Si$^+$ implanted silica than Ge$^+$ implanted silica (Figs. 4.1 and 4.2). Here we see a significant blue B luminescence emission (460 nm ; 2.7 eV) and an intense broad luminescent band in the green-yellow G/Y region with a peak beyond 565 nm (2.2 eV). The ultra violet UV (290 nm ; 4.3 eV) and the red R luminescence (650 nm ; 1.9 eV) are also present but with lower intensity than in pure SiO$_2$. The expectation of another red luminescence at around 750 nm (1.65 eV) is also possible. The only difference between the CL spectra of Si$^+$ and C$^+$ implanted samples are that two additional luminescence bands in UV and V regions are excited. One is at 335 nm (3.7 eV) and the other at around 395 nm (3.1 eV). Luminescence at 335 nm is reported in AlGaN [Riemann et al. 2002], in Lu$_3$Al$_5$O$_{12}$ films [Zorenko et al. 2005] and even in crystalline SiO$_2$ (α-quartz) coated with LiNbO$_3$ [Siu et al. 1999], but never in normal or carbon implanted silica. The violet V luminescence comes into view at a lower wavelength, 394 nm, where this luminescence band was detected in the wavelength range 400-410 nm in other implanted silica layers, as we have already demonstrated in Ge$^+$ implanted SiO$_2$. We found this band in all ion implanted samples which means that the violet luminescence is not only created due to a specific ion kind implanted in silicas but part of it arises from the network damage caused by the ion beam bombardment. Here the intensity of the V band is lower compared to CL spectra of other ion implanted samples presented in this study. We propose that some carbon atoms have been diffused out of the network due to samples thermal treatments.

The intense room-temperature luminescent bands from the blue up to the yellow spectral region as a result of C$^+$ ion-implantation processes into SiO$_2$ layers have been reported by several authors [Zhao et al. 1998, Yu et al. 1998, Rebohle et al. 2001b]. There is a general consensus in assigning these bands to the formation of C-related nanoparticles. The green-yellow luminescence band (2.0-2.2 eV) was also observed in the C$^+$ implanted SiO$_2$ layers. In this case, the intensity of the luminescent band was well correlated with the contribution of carbon-related nanoclusters. A luminescence band at higher energies, in the range of 2.7 eV, has also been reported from carbon graphite-like nanoparticles embedded in SiO$_2$ layers synthesized either by ion implantation [Yu et al. 1998, Gonzalez-Verona et al. 2002] or by

sputtering deposition of C-rich oxides [Zhang et al. 1996] followed by thermal annealing. The blue luminescent band is also characteristic of SiC-related crystalline nanostructures, as porous SiC [Ma et al. 2000]. Furthermore, some authors have analyzed the PL emission from C^+ implanted SiO_2 and they attributed the luminescent bands in the blue region to the formation of amorphous clusters of $Si_yC_{1-y}O_x$ complexes [Rebohle et al.2001b]. The microstructure of carbon implanted silica was investigated by Auger electron spectroscopy (AES) and transmission electron microscopy (TEM). Amorphous nanostructures with a size between 2 and 3.5 nm were found in a depth region between 80 and 150 nm below the oxide surface. Strong photoluminescence (PL) around 2.1 and 2.7 eV has also been observed after excitation at 4.77 eV as an indication of nanoclusters [Rebohle et al. 2001b].

4.4 Tin implantation SiO_2:Sn^+

The implantation of Sn ions into SiO_2 layers has been studied in connection with the formation of defects and nanostructures exhibiting intense visible and ultraviolet Cathodoluminescence (CL). The spectra of Sn^+ implanted SiO_2 is dominated by a strong violet V emission band with the intensity maximum at about 400 nm and a faint shoulder of the blue luminescence at its usual position in SiO_2 spectra (around 460 nm), see Fig. 4.10. It seems that another UV band is overlapped with the UV band detected previously at 290 nm, or it could be that the 290 nm luminescence band has shifted to a higher wavelength position at around 320 nm. An emission band at 320 nm is attributed to bulk tin dioxide [Lopes et al. 2005a, Calestani et al. 2005]. Tin dioxide (SnO_2) is an n-type semiconductor with a wide band gap (E_g=3.6 eV at 300 K) and is particularly important for many electronic applications. At low temperature (10 K) the intensity maximum of the UV band experiences a blue shift of about 10 nm.
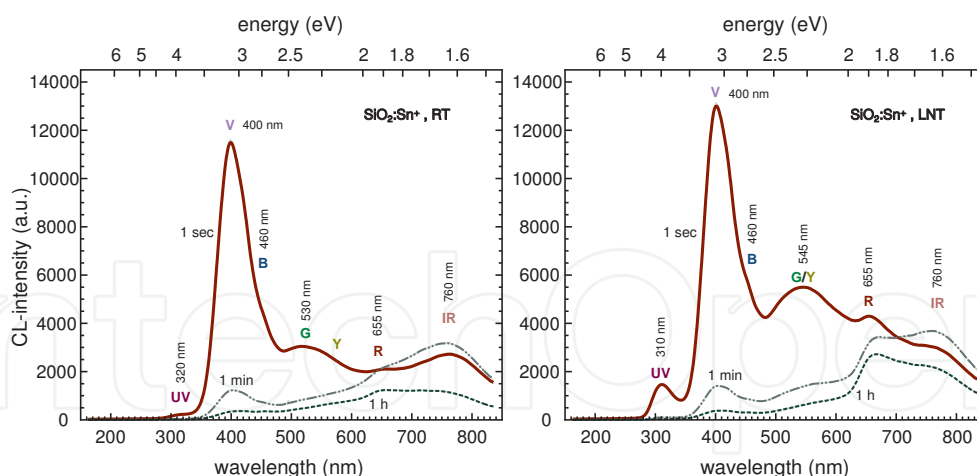

Fig. 4.10 CL-spectra of Sn^+-implanted (500nm) SiO_2 layers (implantation dose D=5×10^{16} cm^{-2}) recorded at RT and LNT. The sample was thermally annealed at T_a=900 °C.

A broad band G peaked at about 530 nm is revealed in room temperature (RT) CL spectra; this band was assigned to Sn nanobelts (or Sn rings) with a lateral dimension 50 nm to 1000 nm. Smaller nanobelts were assigned with longer wavelength position in the CL spectra. At LNT the G/Y shifts 15 nm forward to the red region. In addition, the formation of a rather dense array of Sn-rich nanoparticles presenting a narrow size dispersion and located within the oxide but very close to the SiO_2/Si interface has been observed [Lopes et al. 2005a]. More

Silicon Nanocluster in Silicon Dioxide: Cathodoluminescence,
Energy Dispersive X-Ray Analysis and Infrared Spectroscopy Studies

205

recently, it has been shown that the annealing atmosphere also influences the microstructure development of Sn^+ implanted silica layers, with significant effects in blue-violet PL response [Lopes et al. 2005a]. Sn^+ implanted samples were thermally annealed at T_a=900 °C. The CL bands in the V, B and G regions were associated with oxygen deficiency centers ODC created during the implantation and annealing processes [Rebohle et al. 2000], and probably assisted by the development of the nanoparticles system.

Data from literature [Hu et al. 2002, Hu et al. 2003] report on the evidence of broad PL optical bands from SnO_2 nanobelts in visible wavelength range from 400 nm to 600 nm. The nature of the transition is tentatively ascribed to nanocrystals inside the nanobelts or to Sn or O vacancies occurring during the growth which can induce trapped states in the band gap [Wu et al. 1997]. Other authors [Gu et al. 2003] present absorption and PL luminescence spectroscopy on SnO_2 nanoparticles showing an absorption edge at 300 nm. The same authors show two distinct PL emissions at 400 and 430 nm which are tentatively attributed to Sn interstitials or dangling bonds and to oxygen vacancies respectively.

The indication of the presence of doping-related oxygen deficient centers (ODC's) was obtained from the 5 eV absorption band. This band is supposed to arise from twofold coordinated silicon (=Si) cation sites in pure silica, and =Ge or =Sn sites in Ge^+ doped and Sn^+ implanted silica [Skuja 1992a, Anedda et al. 2001], as evidenced by polarized photoluminescence and lifetime data of the emission excited in this band [Skuja 1992a].

In particular, we showed that Sn^+ doping can give rise to strong and thermally stable luminescence bands. However, it is not clear whether the microscopic mechanisms involved are those proposed to be responsible for the photosensitivity of Sn^+ doped silica photoconversion of optically active defects induced by doping and structural compaction of the doped host network.
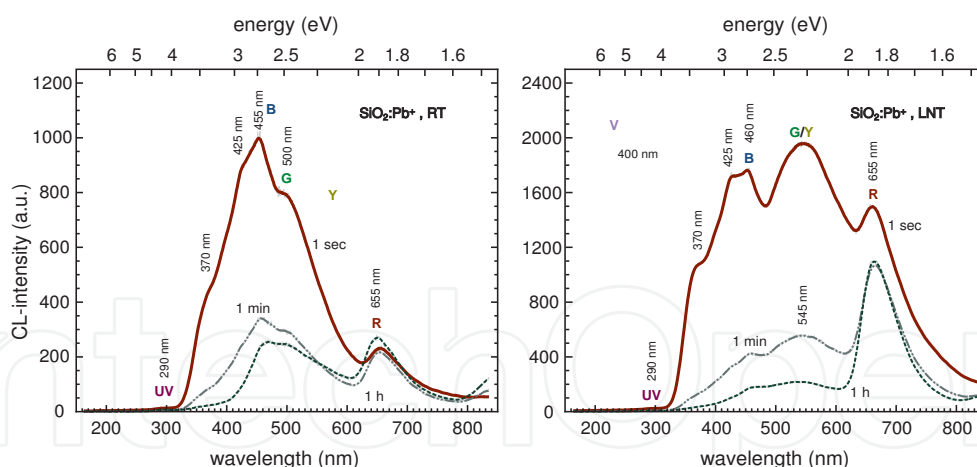

Fig. 4.11 CL-spectra of Pb^+-implanted (500 nm) SiO_2 layers (implantation dose D=5×10^{16} cm^{-2}) recorded at RT and LNT. The sample was thermally annealed at T_a=900 °C.

The red R luminescence (655 nm) is partially eliminated due to Sn^+ implantation. A probable IR CL band can be seen in Fig. 4.10. No evidence of CL or PL emission at 760 nm is, however, reported.

4.5 Lead implantation $SiO_2:Pb^+$

The CL spectrum of the Pb^+ implanted sample is shown in Fig. 4.11. Both Sn and Pb are classified as metallic substances in contrast to the other dopands presented in this section.

Pb^+ implantation creates defect centers providing more intense luminescence in the violet-blue region. Here, two UV bands are detected; one is the UV of the SiO_2 matrix at 290 nm with very low intensity and another, for sure due to Pb implantation at 370 nm. Contrary to the violet band detected in Ge and Sn implanted silicas, the violet band in Fig. 4.11 is shifted towards longer wavelengths (425 nm) and showing lower intensity than the blue luminescence at 455 nm. We were anticipating the existence of a luminescence band at exactly at 500 nm and even in pure SiO_2. Pb^+ implantation enhanced this band significantly at RT. The blue and the green bands suffered red shifts when the measurement's temperature was changed to LNT.

All bands labeled in Fig. 4.11 were going through destructive modes where their intensities dropped considerably in the first seconds of irradiation and they never recovered again as it is often happens in pure SiO_2 CL spectra. The bands in the shorter wavelength than the red are often ascribed to nucleation of the dopand atoms in silica, therefore we expect different forms of Pb aggregates which destroyed under the electron beam irradiation, can be the main precursor of these bands.

The famous red band (655 nm) has lost fractions of its intensity because of Pb^+ implantation but it goes via destructive and creation modes simultaneously, where the NBOHC is saturated by the dopands and followed by liberation from the dangling oxygen bonds under heavy electron bombardment.

5. Group VI elements implanted in SiO_2

The visible cathodoluminescence from Si and its substitutional atoms at room temperature and liquid nitrogen temperatures have been presented in the previous section. In this section we will report the luminescence emission characterizing oxygen ion-implantation in a-SiO_2 layers under electron beam excitation. Moreover some other elements (sulfur and selenium) from group IV which are supposed to replace some of the oxygen atoms in the silica matrix are important for better understanding of oxygen related radiation processes and the structure and electronic state of respective defects while oxygen diffusion and chemistry in SiO_2 are most important for silicon-based microelectronics.

5.1 Oxygen implantation SiO_2:O^+

The typical CL spectra of wet SiO_2 is dominated mainly by bands: red R (650 nm, 1.9 eV), blue B (460 nm, 2.7 eV), and UV (290 nm, 4.3 eV) besides we recognize a yellow band Y (570 nm, 2.2 eV) at LNT decaying very rapidly at the beginning of the electron beam irradiation and CL excitation, but appearing and increasing at RT after a longer time of irradiation. We could relate some of these bands to special luminescence defect centers. Defects rolled or influenced by addition of oxygen are shown in Fig. 5.1 where the CL spectra of an oxygen implanted SiO_2 layer are presented. Direct comparison between Fig. 5.1 and the CL on non-implanted (pure) SiO_2 shows that the changes are in the red luminescence region and no extra modification in the other regions of the spectra. This serves to confirm the origin and the structure of the NBOHC where more strained silicon-oxygen bonds can transfer to $\equiv$Si$-$O$\bullet$ and more interstitial oxygen can be produced depending on the implantation doses. The red luminescence is not only associated with the NBOHC but also associated with interstitial oxygen [Skuja et al. 1994a].
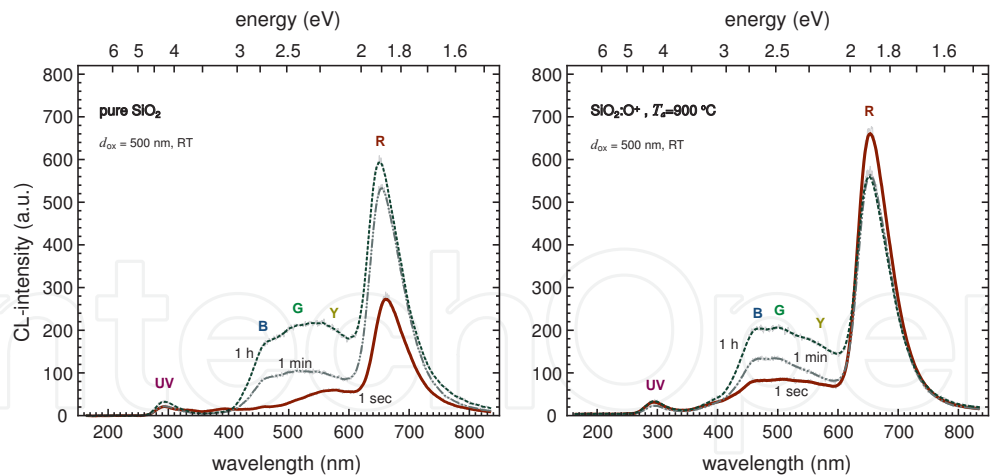
Silicon Nanocluster in Silicon Dioxide: Cathodoluminescence,
Energy Dispersive X-Ray Analysis and Infrared Spectroscopy Studies

207

Fig. 5.1 CL spectra of non-annealed and annealed (T_a=900 °C) O$^+$ implanted SiO$_2$ layers at room temperature (RT). The initial spectra are labeled by (1 sec) and the saturated by (1 h).

5.2 Selenium implantation SiO$_2$:Se$^+$

Se$^+$ was isoelectrically implanted with regard to oxygen. Fig. 5.2 shows the CL spectra obtained from the SiO$_2$ layers implanted by Se$^+$ and annealed at 900 °C. Once again no change is found in the UV luminescence; it is appearing at the same position with low intensity, also the violet luminescence due to Se implantation this time at 410 nm. The blue luminescence is also located clearly at 460 nm. The red and yellow luminescences are enhanced by Se$^+$ implantation, and both bands seem to be from the same origin as in pure SiO$_2$ where both have the same tendency during electron beam irradiation at RT and LNT.
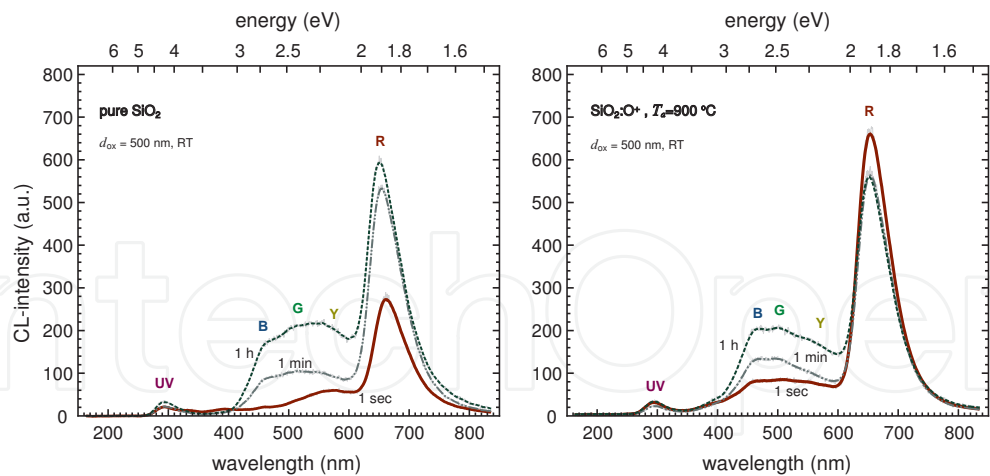

Fig. 5.2 CL spectra of non-annealed and annealed (T_a=900 °C) Se$^+$ implanted SiO$_2$ layers at room temperature (RT) and liquid nitrogen temperature (LNT). The initial spectra are labeled by (1 sec) and the saturated by (1 h).

5.3 Sulfur implantation SiO$_2$:S$^+$

Defect centers in sulfur-implanted silica layers differ considerably from those observed in other implanted samples. Fig. 5.3 shows the cathodoluminescence spectra of S$^+$ doped SiO$_2$ at room temperature (RT) and liquid nitrogen (LNT) as well as their time dependence.

Obviously, the high violet intensity V at ≈405 nm is assigned to sulfur S$^+$ implantation. Moreover, a sharp and intensive multi-step emission in the green-yellow-red-nearIR (500-820 nm) region is observed for these layers. The exact band positions in wavelengths and energies are given in Table 5.1.

The UV band (290 nm) has been observed at the same position in both samples as well as in pure SiO$_2$. Moreover, after longer irradiation of about 1 min, i.e. an electron beam dose of 0.3 As/cm^2, the multiplet structure disappears and the characteristic red band R (660 nm) of the NBOHC in SiO$_2$ becomes visible besides remaining components at the blue band B (460 nm) position and in the yellow region at 560 nm and 590 nm. On the other hand, the sulfur-associated violet band V (405 nm) still remains visible.

Analyzing the multiplet (MP) band structure according to the data listed in Table 5.1, we find that the energy differences between the sub-bands start from 0.14 eV in the green region and then decreases to 0.12 eV in the red region up to 0.11 eV in the near IR. Thus the mean step width amounts to about 120 meV. This energy difference may correspond to a series of almost equidistant vibration levels of non-saturated sulfur radicals ≡Si−S• or ≡Si−O−S• formed during implantation and thermal annealing analogously to the red R band center of the non-bridging oxygen (NBOHC) ≡Si−O• in pure SiO$_2$.
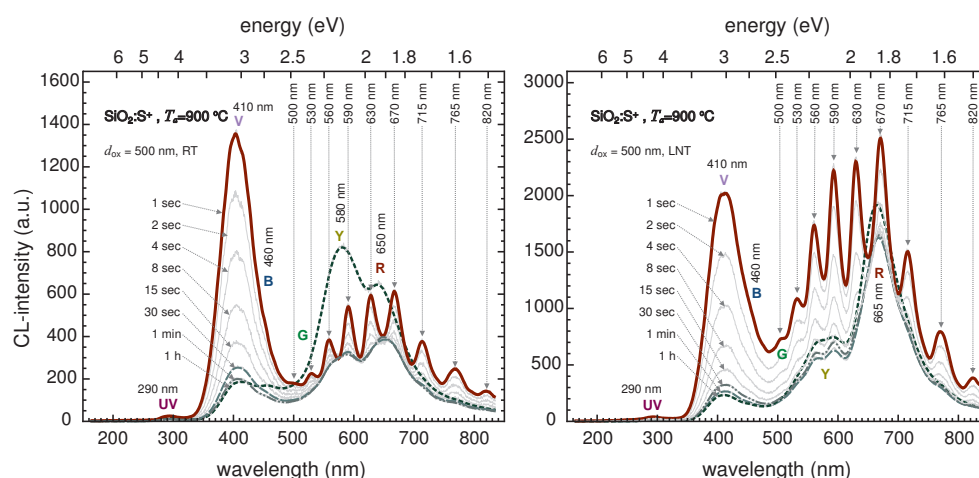

Fig. 5.3 CL spectra of non-annealed and annealed (T_a=900 °C) S$^+$ implanted SiO$_2$ layers at room temperature (RT) and liquid nitrogen temperature (LNT). The initial spectra are labeled by (1 sec) and the saturated by (1 h).

Even the MP step widths decrease with lower photon energy, beginning with ΔE=140 meV at hν=2.48 eV and dropping to ΔE=110 meV at hν=1.51 eV, indicating a widened (sub-quadratic) potential curve of the luminescence ground states with compressed higher vibration levels imagined in terms of the adiabatic configuration coordinate model.

5.4 Investigation of the multimodal luminescence

Before attributing this effect to sulfur implantation, we should prove whether the structured spectrum is indeed true or arises from some experimental artifacts. We considered the second argument in our first analysis, where contaminated layers especially at low temperature measurements, interference (Fabry-Perot type) in thin films, and monocrystals as quantum dots could also cause such effects temporarily. The measurements of the CL spectra of the S$^+$ implanted sample have been repeated many times and under different

Silicon Nanocluster in Silicon Dioxide: Cathodoluminescence,
Energy Dispersive X-Ray Analysis and Infrared Spectroscopy Studies

209

experimental conditions; the results were always the same. Samples annealed at higher temperatures still showed resolved multimodal bands, see Fig. 5.4, but the structured area was less sharp, indicating a destruction of the centers causing this effect. Then any experimental artifacts are definitely excluded.

Cluster formation is always expected especially when the samples are annealed at temperatures exceeding 900 °C. We found no traces of sulfur clusters in our samples. Fig. 5.5 shows a STEM micrograph of the S^+ implanted silica layer in the same magnification as used to detect Ge cluster (Fig. 5.4). S^+ implanted silica is rarely reported in the literature. Some authors reported their PL results of S^+ doped in 1 mm thick optical fiber disks; the sulfur content was 0.05 wt% which corresponds to 2×10^{19} atoms/cm³. They attributed a similar structured luminescence spectra but at a lower energy region (300-500 nm) to S_2 and S^+_2 interstitial molecules [Zavorotny et al. 2001, Gerasimova et al. 2002]. But afterwards they concluded that the irregular intensity distribution of vibrational components of the PL excitation band indicates that the color centers responsible for this band belong not to a diatomic molecule with one vibrational frequency but to a polyatomic molecule whose vibrational spectrum is formed by a combination of three vibrational frequencies.

	SiO₂				SiO₂ :S		
	λ/nm	$h\nu$/eV			λ/nm	$h\nu$/eV	ΔE/meV
UV	290	4.3		UV	290	4.30	
B	460	2.7		V	405	3.10	
Y	570	2.2			500	2.48	
R	660	1.9			530	2.34	140
				Y	560	2.21	130
					590	2.10	110
				MP	630	1.97	130
				R	670	1.85	120
					715	1.73	120
					765	1.62	110
				IR	820	1.51	110

Table 5.1 Luminescence bands and multiplet states (MP) in SiO₂ and sulfur implanted SiO₂:S.

It is for this reason that they later attempted the multimodal structured spectra with the SO₂ molecule [Gerasimova 2003]. Whether this hypothesis is correct or not, we see a direct connection between the multimodal structured luminescence and oxygen atoms where sulfur atoms are supposed to substitute oxygen in the matrix and then more oxygen in interstitial sites is expected because over-stoichiometric SiO_x with $x>2$ does not exist.
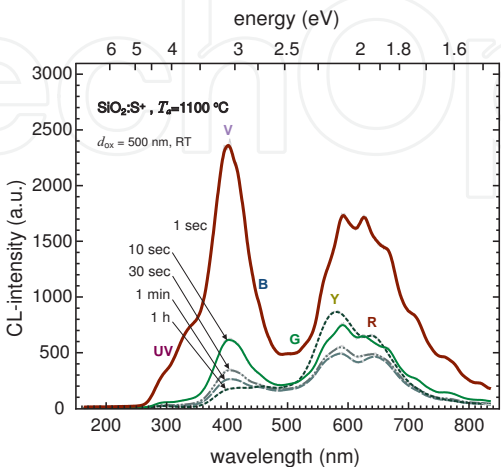

Fig. 5.4 Room temperature (RT) CL spectra of annealed S^+ implanted SiO₂ at higher temperature (T_a=1100 °C).
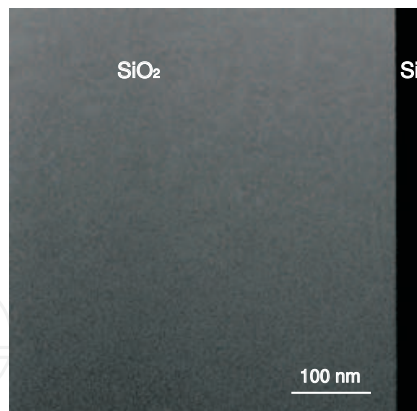
Fig. 5.5 STEM micrograph of the S$^+$ implanted silica layer annealed at 900 °C showing no evidence of sulfur clusters.

In order to avoid water formation and binding of oxygen we have chosen dry oxidized SiO$_2$ layers to run our test. Oxygen atoms were implanted in a thinner (d_{ox}=100 nm) dry SiO$_2$ layer with lower energy (20 keV) and lower doses (3×10^{16} cm^{-2}). Thus the overall CL intensity is about one order of magnitude lower than in 500 nm thick wet oxidized layers, Fig. 5.6. Surprisingly we found the same multiple regular-shaped structure from the green G over the yellow Y and red R regions into near infrared IR in the same peak positions, when the sample was annealed at 1000 °C. And no trace of the violet luminescence was to be seen, see Fig. 5.6. Such structural spectra are never recorded even by using different compositions of non-implanted SiO$_2$ layers.

This leads us to the conclusion that not sulfur but oxygen should be the source of these multimodal spectra. As already declared, oxygen is responsible for the red R luminescence in SiO$_2$.

Looking to the literature, we found excitation [Rolfe 1979] and emission spectra [Ewig and Tellinghuisen 1991] of the negatively charged oxygen molecule O$^-_2$ on interstitial sites in alkali halide crystals. The ground electronic state and several low-lying excited states of the superoxide ion O$^-_2$ have been studied by multi-configuration self-consistent fields (MCSCF), see Fig. 5.7. For comparison, the ground state of the neutral O$_2$ molecule was also considered. Parallel computations were carried out for the species in vacuo and in a simulated KCl crystal lattice (in lattio). Computed spectroscopic parameters are in good agreement with experiments for X and A states of O$^-_2$ in vacuo. In Fig. 5.7 there is also substantial agreement between the computed energy curves for both the ground X and the excited A states in a point-charge lattice and those measured in alkali halide lattices. Further, the spectroscopic parameters of the electron scattering resonance states in vacuo agree well with those of the analogous lattice-stabilized excited electronic states in the solid. There is a typical absorption from the ground state X to the excited state A of about hν=5.1 eV corresponding to the red R luminescence excitation associated with the NBOHC [Skuja 1994a]. Moreover, the related luminescent transition from $A{\rightarrow}X$ shows the red R luminescence at about hν=2 eV. Looking to vibronic levels within the potential configuration curves, we see levels of about 120 meV step-widened towards higher energies, i.e towards the green G region, Fig. 5.7. Thus we should prefer the explanation of the multimodal spectra by means of electronic-vibronic spectra transitions as given by the common configuration coordinate model of luminescence. All transitions appear in good agreement with the multimodal CL spectra of SiO$_2$:O and SiO$_2$:S layers shown here. Therefore we favor

Silicon Nanocluster in Silicon Dioxide: Cathodoluminescence,
Energy Dispersive X-Ray Analysis and Infrared Spectroscopy Studies

211

the interstitial O^-_2 model for the multimodal CL structure and may reject the concept of a photonic crystal structure as proposed in [Bailey et al. 2005] as well as effects of quantum confinement as reported recently for GaAs quantum dots in [Rodt et al. 2005]. Of course, in the latter case of GaAs or other nanostructure materials even other molecule formations should be taken into account as possibly responsible for different but similarly shaped multimodal structures of luminescence spectra.
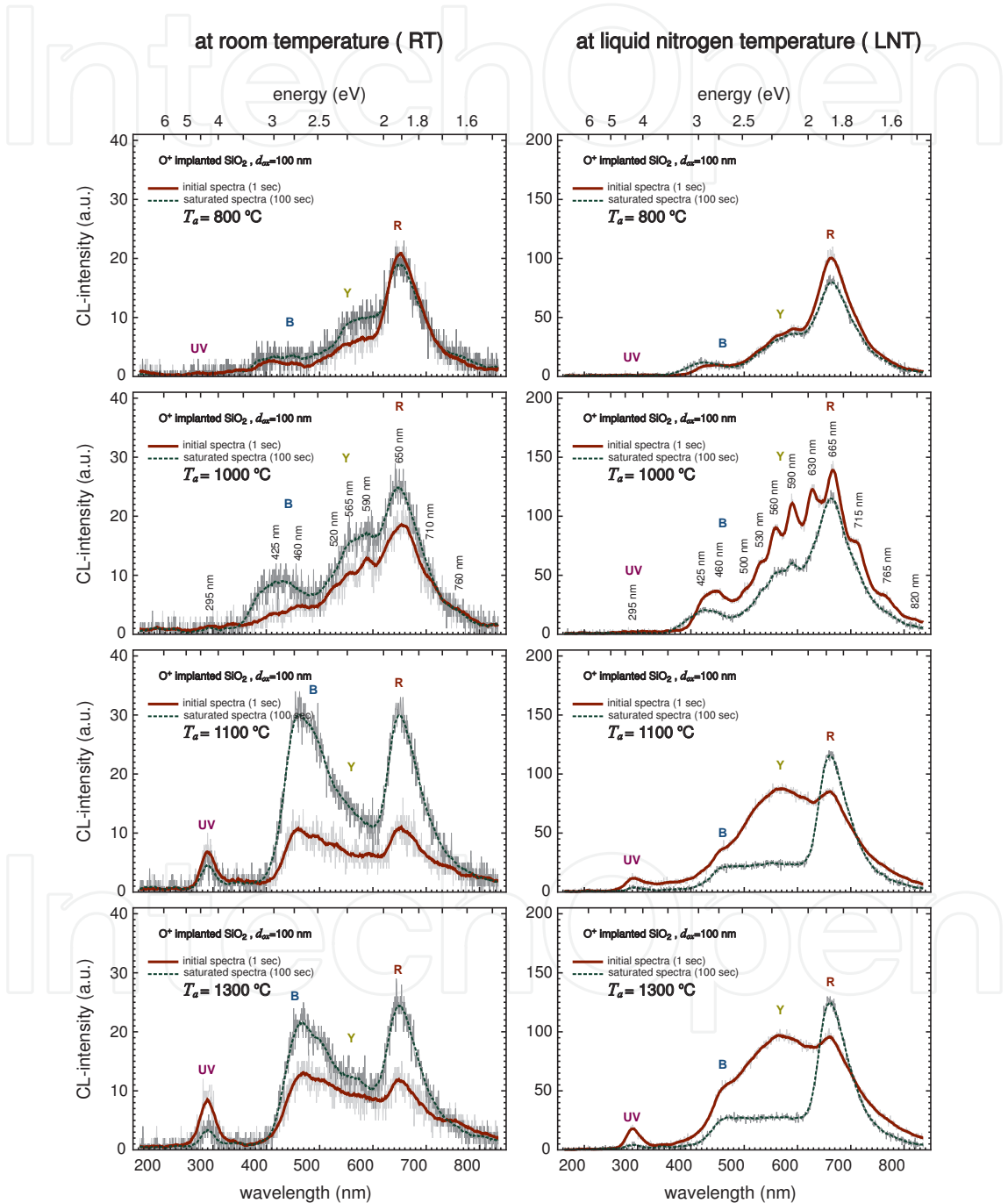

Fig. 5.6 CL spectra of non-annealed and annealed (T_a=700, 900, 1000, 1300 °C) O+ implanted SiO$_2$ layers at room temperature (RT) and liquid nitrogen temperature (LNT). The initial spectra are labeled by (1 sec) and the saturated by (1 h).
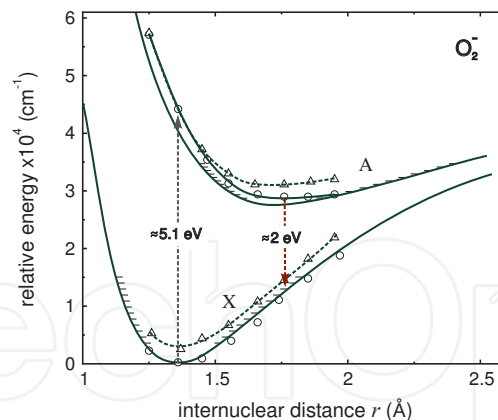
Fig. 5.7 Comparison of MCSCF in lattio (cycles) and in vacuo (triangles) energies with experimental Morse curves derived from analysis of absorption, excitation and luminescence spectra of O^-_2 in NaCl; vibronic levels are indicated by bars [Ewig and Tellinghuisen 1991]

6. Conclusions

The investigation of the present work are extended to various electronical and optical modifications of silica SiO_2 layers as they are applied in microelectronics, optoelectronics, as well as in forthcoming photonics. Electron irradiation of a-SiO_2 layers induces chemical defect reactions dependent on the sample oxidation procedure, thermal post-annealing and CL excitation temperature. The red luminescence R (650 nm ; 1.9 eV) is associated with the non-bridging oxygen hole center (NBOHC: ≡Si−O•) whereas the blue luminescence B (460 nm ; 2.7 eV) and the ultraviolet band UV (4.2 eV ; 295 nm) are attributed to Si-related oxygen deficient centers (Si-ODC). CL spectra of hydrogen-free (dry-oxidized) and hydrogen-rich (wet-oxidized) samples have shown significant differences especially in the red region. Hydrogen and hydroxyl groups during wet oxidization increase the intensity of the red luminescence center, where exposure of SiO_2 during the oxidation to water vapor results in the appearance of various OH species (Si−O−H, hydrogen bonded OH, H_2O and the Si−H bond). Thus the dose-dependence of the red R luminescence in wet and dry oxides differs significantly, decreasing in wet oxide from a high initial level down to saturation and increasing in dry oxide from almost zero to saturation. The initial decrease in the red luminescent NBOHC concentration is indicating a recombination of NBOHC with different types of hydrogenous species. In dry SiO_2 the strained bonds (≡Si−O··Si≡) and their electron beam-induced rupture are the precursors for the NBOHC. The mean lifetime of the red luminescence in wet oxide τ=(4.7±0.2)µs is almost the same as in dry oxide τ=(5.3±0.2)µs. Additional hydrogen ion implantation into SiO_2 diminishes the intensity of the red luminescence R because of hydrogen saturation of NBOHC, but magnifies the yellow luminescence Y to very high intensity, even higher than the intensity of the red luminescence. In hydrogen implanted SiO_2 the yellow Y luminescence appears after irradiation doses of about 2 As/cm² and we may propose that this band is due to water molecules in the SiO_2 network formed by mobile radiolytic hydrogen and oxygen. A comparison with the CL of water (ice) layers supports this hypothesis.

Understoichiometric SiO_x layers with x≤2 of oxygen deficit or silicon surplus are prepared by means of thermal evaporation of silicon monoxide SiO_1 in different ambient oxygen

Silicon Nanocluster in Silicon Dioxide: Cathodoluminescence,
Energy Dispersive X-Ray Analysis and Infrared Spectroscopy Studies

213

atmospheres. The stoichiometric degree varies between $1 \leq x \leq 2$ and was determined by FTIR calibration measurements by means of the respective shift of the Si−O−Si stretching mode. CL spectra of SiO_x begin to show first typical silica luminescence bands at a stoichiometric threshold of about $x>1.4$. Thermal annealing of these layers and electron bombardment lead to a partial phase separation of SiO_x into atomic Si fragments and clusters in a nearly stoichiometric SiO_2 matrix. This process is correlated with the different luminescent centers in amorphous SiO_2. Especially the yellow luminescence 2.1 eV seems to be associated with silicon hexamer rings in under-stoichiometric SiO_x. Probably they represent the first step of Si nanocrystal formation. Further on, Si clusters can grow to a size of several nanometers. The size distribution, shown by TEM micrographs, exhibits a most probable diameter size of 4 nm and a maximum diameter up to 10 nm. Our results provide evidence that at least two distinct defects are responsible for the yellow luminescence Y at 2.1 eV in silica. The first in wet and H-implanted SiO_2 is due to high H_2O molecule content which can be removed by thermal annealing until it behaves like normal wet SiO_2. The second defect for the yellow luminescence in dry SiO_2 (where almost no H or H_2O exist) could be due to oxygen deficient centers in the form of silicon fragments or small rings in the SiO_2 network.

To investigate whether the different luminescent centers are related to oxygen or to silicon, we have compared non-stoichiometric SiO_2 layers produced by direct oxygen or silicon ion implantation. Thermally oxidized SiO_2 layers of 100 and 500 nm thickness have been implanted with different kinds of ions with a dose 3×10^{16} and 5×10^{16} ions/cm^2, respectively, leading to an atomic dopant fraction of about 4 at.% in the middle, i.e. the half depth of the SiO_2 layers. Oxygen implantation as well as, on the other hand, direct silicon implantation led to an oxygen surplus as well as an oxygen deficit, respectively. As the main experimental results we could state: Oxygen surplus increases the red band R in SiO_2 but does not affect the blue band B. Silicon surplus increases the blue luminescence B, but reduces the red band R. So it is verified that the red luminescence R is an oxygen related center stated as NBOHC and the blue luminescence B is a silicon related oxygen deficient center Si-ODC.

In Ge$^+$-implanted SiO_2 a huge violet band V (3.1 eV ; 410 nm) appears and is associated with the Ge-related oxygen deficient center Ge-ODC. It dominates the luminescence spectra, covering the original blue band B (Si-ODC) of the SiO_2 matrix. Further on, the V band shows a large increase after thermal annealing. Thus thermal annealing around temperatures of T_a=900 °C increases the violet luminescence of the Ge-ODC by more than two orders of magnitude. Thus the Si-ODC's as well as the Ge-ODC's are formed by Si and Ge molecules clustering to certain low-dimension fragments: dimers, trimers and higher aggregates. With further annealing at higher temperatures, Si and Ge nanocrystals are formed embedded in the amorphous SiO_2 matrix, and the blue B and the violet V luminescence begin to decrease again. The nanocluster size grows with annealing temperature from 2-4 nm at T_a=900 °C to 5-10 nm at T_a=1100 °C.

Further on, heavy electron beam bombardment of SiO_2 with doses of 2.7 As/cm^2 and associated oxygen dissociation may also create Si nanoclusters in a size range of 2-10 nm with a most probable diameter of 4 nm. These Si nanoclusters with their quantum confinement are a source of luminescence in the near IR at 1.6 eV and probably at 1.3 eV too. Further ion implantations of group IV elements: C$^+$, Sn$^+$, Pb$^+$ which are thought to substitute Si in the silica matrix, show new bands and a general increase of the luminescence in the blue region. On the other hand, implantations of oxygen substitute elements of group VI

lead to an increase in the red spectral region. The ultraviolet UV and violet V luminescence are detected in mostly all ion implanted samples at around 290 nm and 410 nm, respectively, indicating not only extrinsic related ODC or extrinsic defects but also ion implantation induced defects in the SiO_2 matrix.

As a surprising peculiarity, the cathodoluminescence spectra of oxygen and sulfur implanted SiO_2 layers show, besides characteristic bands, a sharp and intensive multimodal structure beginning in the green region at 500 nm over the yellow-red region and extending to the near IR measured up to 820 nm. The energy step differences of the sublevels amount to an average of 120 meV and indicate vibronic-electronic transitions, probably, of O_2^- interstitial molecules, as we could demonstrate by a respective configuration coordinate model. However, such "mysterious" multimodal luminescence spectra are observed occasionally in other material compounds too, and are many-fold in their interpretations by other authors ranging from photonic crystals and interference effects over discrete quantum dots and respective quantum confinement, even to our model of interstitial molecules and their electronic-vibronic luminescent transitions.

7. References

Anedda A. , Carbonaro C. M. , Serpi A. , Chiodini N. , Paleari A. , Scotti R. , Spinolo G. , Brambilla G. and Pruneri V. : *Vacuum ultraviolet absorption spectrum of photorefractive Sn-doped silica fiber preforms*, J. Non-Cryst. Solids 280 (2001) 287.

Anedda A. , Carbonaro C. M. , Clemente F. , Corpino R. , Grandi S. , Mustarelli P. and Magistris A. : *OH-dependence of ultraviolet emission in porous silica*, J. Non-Cryst. Solids 322 (2003b) 68.

Bailey R. C. , Parpia M. , Hupp J. T. : *Sensing via optical interference*, Materialstoday, Vol 8, Iss.4, April (2005), 46.

Bakaleinikov L. A. , Zamoryanskaya M. V. , Kolesnikova E. V. , Sokolov V. I. and Flegontova E. Yu. : *Silicon Dioxide Modification by an Electron Beam*, Physics of the Solid State 46 (2004) 1018.

Bakos T. , Rashkeev S. N. and Pantelides S. T. : *H_2O and O_2 molecules in amorphous SiO_2:Defect formation and annihilation mechanisum* , Phys. Rev. B 69 (2004a) 195206.

Bakos T. , Rashkeev S. N. and Pantelides S. T. : Optically active defects in SiO_2: *The nonbridging oxygen center and interstitial OH molecule*, Phys. Rev. B 70 (2004b) 75203.

Barfels T. : PhD dissertation , *Kathodolumineszenz amorpher und kristalliner Modifikationen von SiO_2 und GeO_2*, Rostock university (2001).

Blöchl P. E. : *First-principles calculations of defects in oxygen-deficient silica exposed to hydrogen*, Phys. Rev. B 62 (2000) 6158.

Brichard B. , Fernandez A. F. , Ooms H. , Borgermans P. and Berghmans F. : *Dependence of the POR and NBOHC Defects as Function of the Dose in Hydrogen-Treated and Untreated KU1 Glass Fibers*, IEEE Transactions on Nuclear Science 50 (2003) 2024.

Calestani D. , Lazzarini L. , Salviati G. and Zha M. : *Morphological, structural and optical study of quasi-1D SnO_2 nanowires and nanobelts*, Cryst. Res. Technol. 40 (2005) 937.

Cannas M. , Agnello S. , Boscaino R. , Costa S. , Gelardi F. M. , Messina F. : *Growth of H(II) centers in natural silica after UV laser exposure*, J.Non-Cryst. Solids, 322 (2003b) 90.

Cazaux J. : *Some considerations on the electric field induced in insulators by electron bombardment* , J. Appl. Phys. 59 (1986) 1418.

Silicon Nanocluster in Silicon Dioxide: Cathodoluminescence,
Energy Dispersive X-Ray Analysis and Infrared Spectroscopy Studies

215

Ewig C. S. and Tellinghuisen J. : *Ab initio study of the electronic states of O^-_2 in vacuo and in simulated ionic solids*, J. Chem. Phys. 95 (1991) 1097.

Fitting H.-J. , Barfels T. , Trukhin A. N. , Schmidt B. , Gulans A. and von Czarnowski A. : *Cathodoluminescence of Ge^+, Si^+, and O^+ implanted SiO_2 layers and the role of mobile oxygen in defect transformation*, J. Non-Cryst. Solids 303 (2002b) 218.

Fitting H.-J. , Ziems T. , von Czarnowski A. and Schmidt B. : *Luminescence center transformation in wet and dry SiO_2*, Radiation Measurements 39 (2004) 649.

Fitting H.-J. , Ziems T. , Salh R. and von Czarnowski A. : *Luminescent defect dynamics in amorphous SiO_2:H*, phys. stat. sol. (c) 2 (2005a) 693.

Fitting H.-J. , Ziems T. , Salh R. , Zamoryanskaya M. V. , Kolesnikova K. V., Schmidt B. and von Czarnowski A. : *Cathodoluminescence of wet, dry and Hydrogen-implanted silica films*, J. Non-Cryst. Solids 351 (2005b) 2251.

Fitting H.-J. , Salh R. , Barfels T. and Schmidt B. : *Multimodal Luminescence Spectra of Ion-implanted Silica*, phys. stat. sol. (a) 202 (2005c) R142.

Gerasimova V. I. , Zavorotny Yu. S. , Rybaltovskii A. O. , Chernov P. V. , Sazhin O. D. , Khrapko R. R. and Frolov A. A. : *Color Centers in Sulfur-Doped Silica Glasses: Spectroscopic Manifestations of an S^+_2 Interstitial Molecular Ion*, Glass Physics and Chemistry 28 (2002) 5.

Gerasimova V. I. , Rybaltovskii A. O. , Chernov P. V. and Spasskii D. A. : *Color Centers in Sulfur-Doped Silica Glasses: Spectroscopic Manifestations of an SO_2 Interstitial Molecule*, Glass Physics and Chemistry 29 (2003) 232.

Goldberg M. : *Cathodoluminescence and cathode-electroluminescence of SiO_2-layers*, PhD thesis, University of Rostock, (1996).

Gonzalez-Verona O. , Garrido B. , Perez-Rodriguez A. , Morante J. R. , Bonafos C., Carrada M., Sanz L. F. , Gonzalez M. A. and Jimenez J. : *Analysis of the white emission from ion beam synthesised layers by in-depth resolved scanning photoluminescence microscopy*, Materials Science and Engineering B 91 (2002) 51.

Griscom D. L. : *Electron spin resonance investigations of defects and defect processes in amorphous silicon dioxide*, Rev. Solid State Sci. 4 (1990b) 565.

Gu F. , Wang S. F. , Song C. F. , Lu M. K. , Qi Y. X. , Zhou G. J. , Xu D. and Yuan D. R. ; *Synthesis and luminescence properties of SnO_2 nanoparticles*, Chem. Phys. Lett. 372 (2003) 451.

Helm C. R. and Deal B. E. (eds.) : *The Physics and Chemistry of SiO_2 and the Si-SiO_2 Interface*, Plenum, New York, (1993).

Hosono H. , Weeks R. A. , Imagawa H. and Zuhr R. : *Formation of oxygen-deficient type structural defects and state of ions in SiO_2 glasses implanted with transition metal ions*, J. Non-Cryst. Solids 120 (1990) 250.

Hu J. Q. , Ma J. X. L. , Shang N. G. , Xie Z. Y. , Wong N. B. , Lee C. S. and Lee S. T.: *Large-Scale Rapid Oxidation Synthesis of SnO_2 Nanoribbons*, J. Phys. Chem. B 106 (2002) 3823.

Hu J. Q. , Bando Y. and Golberg D. : *Self-catalyst growth and optical properties of novel SnO_2 fishbone-like nanoribbons*, Chem. Phys. Lett. 372 (2003) 758.

Iacona F., Franzo G. and Spinella C. : *Correlation between luminescence and structural properties of Si nanocrystals*, J. Appl. Phys. 87 (2000) 1295

Ivanda M. , Clasen R. , Hornfeck M. and Kiefer W. : *Raman spectroscopy on SiO_2 glasses sintered from nanosized particles*, J. Non-Cryst. Solids 322 (2003) 46.

Kajihara K. , Skuja L. , Hirano M. and H. Hosono : *Diffusion and Reactions of Hydrogen in F₂-Laser-Irradiated SiO₂ Glass*, Phys. Rev. Lett. 89 (2002) 135507.

Kolesnikova E. V. , Sitnikova A. A. , Sokolov V. I. and Zamoryanskaya M. : *Modification of Silicon Oxide by High Energy Electron Beam*, Solid State Phenomena 108-109 (2005) 729.

Kuzuu N. and Horikoshi H. : *X-ray induced absorption in fused silica containing various amounts of OH*, J. Appl. Phys. 97 (2005) 93508.

Ledoux G. , Gong J. , Huisken F. , Guillois O. and Reynaud C. : *Photoluminescence of size-separated silicon nanocrystals: Confirmation of quantum confinement*, Appl. Phys. Lett. 80 (2002) 4834.

Legrand A. P. : *The Surface Properties of Silica*, New York, Wiley, (1998).

Lehmann A. , Schumann L. and Hübner K. : *Optical Phonos in Amorphous Silicon Oxides*, phys. stat. sol. (b) 121 (1984) 505.

Lopes J. M. J. , Zawislak F. C. , Fichtner P. F. P. , Papaleo R. M. , Lovey F. C. , Condo A. M. and Tolley A. J. : *Formation of epitaxial β-Sn islands at the interface of SiO₂/Si layers implanted with Sn ions*, Appl. Phys. Lett. 86 (2005a) 191914.

Lopes J. M. J. , Zawislak F. C. , Fichtner P. F. P. , Lovey F. C. and Condo A. M. : *Effect of annealing atmosphere on the structure and luminescence of Sn-implanted SiO₂ layers*, Appl. Phys. Lett. 86 (2005b) 023101.

Lou V. , Sato R. and Tomozawa M. : *Hydrogen diffusion in fused silica at high temperatures*, J. Non-Cryst. Solids 315 (2003) 13.

Ma T., Xu J. , Du J. , Li W. , Huang X. and Chen K. : *Full color light emission from amorphous SiCx:H with organic-inorganic structures*, J. Appl. Phys. 88 (2000) 6408.

Magruder R. H. , Weeks R. A. and Weller R. A. : *Luminescence and absorption in type III silica implanted with multi-energy Si, O and Ar. ions*, J. Non-Cryst. Solids 322 (2003) 58.

Minke M. V. and Jackson K. A. : *Diffusion of germanium in silica glass* , J. Non-Cryst. Solids 351 (2005) 2310.

Mischler C. , Horbach J. , Kob W. and Binder K. : *Water adsorption on amorphous silica surfaces: a Car-Parrinello simulation study*, J. Phys.: Condens. Matter 17 (2005) 4005.

Morimoto Y. , Weeks R. A. , Barnes A. V. , Tolk N. H. and Zuhr R. A. : *The effect of ion implantation on luminescence of a silica*, J. Non-Cryst. Solids 196 (1996) 106.

Morimoto Y. and Nozawa S. : *Effect of Xe₂ light (7.2 eV) on the infrared and vacuum ultraviolet absorption properties of hydroxyl groups in silica glass*, Phys. Rev. B 59 (1999) 4066.

Mutti P., Ghislotti G. , Bertoni S. , Bonoldi L. , Cerofolini G. F. , Meda L. , Grilli E. and Guzzi M. : *Room-temperature visible luminescence from silicon nanocrystals in silicon implanted SiO₂ layers*, Appl. Phys. Lett. 66 (1995) 851.

Nicklaw C. J. , Pagey M. P. , Pantelides S. T. , Fleetwood D. M. , Schrimpf R. D. , Galloway K. F. , Wittig J. E. , Howard B. M. , Taw E., McNeil W. H. and Conley J. F. , Jr. : *Defects and Nanocrystals Generated by Si Implantation into a-SiO₂*, IEEE Transactions on Nuclear Science 47 (2000) 2269.

Ogasawara H. , Brena B. , Nordlund D. , Nyberg M. , Pelmenschikov A. , Pettersson L.G.M. and Nilsson A. : *Structure and Bonding of Water on Pt(111)*, Phys. Rev. Lett. 89 (2002) 276102.

Pacchioni G. and Mazzeo C. : *Paramagnetic centers in Ge-doped silica: A first-principles study*, Phys. Rev. B 62 (2000) 5452.

Silicon Nanocluster in Silicon Dioxide: Cathodoluminescence,
Energy Dispersive X-Ray Analysis and Infrared Spectroscopy Studies

217

Pan B. C. and Biswas R. : *Simulation of hydrogen evolution from nano-crystalline silicon*, J. Non-Cryst. Solids 333 (2004) 44.

Perez-Rodriguez A. , Gonzalez-Varona O. , Garrido B. , Pellegrino P. , Morante J. R., Bonafos C. , Carrada M. and Claverie A. : *White luminescence from Si^+ and C^+ ion-implanted SiO_2 films*, J. Appl. Phys. 94 (2003) 254.

Prokes S. M. , Carlos W. E., Veprek S. and Ossadnik C. : *Defect studies in as-deposited and processed nanocrystalline Si/SiO_2 structures*, Phys. Rev. B 58 (1998) 15632.

Rashkeev S. N. , Fleetwood D. M. , Schrimpf R. D. and Pantelides S. T. : *Defect Generation by Hydrogen at the $Si-SiO_2$ Interface*, Phys. Rev. Lett. 87 (2001) 165506.

Rebohle L. , von Borany J. , Fröb H. and Skorupa W. : *Blue photo- and electroluminescence of silicon dioxide layers ion-implanted with group IV elements*, Appl. Phys. B 71 (2000) 131.

Rebohle L. , Gebel T. , Fröb H. , Reuther H. and Skorupa W. : *Ion beam processing for Si/C-rich thermally grown SiO_2 layers: photoluminescence and microstructure*, Appl. Surf. Sci. 184 (2001b) 156.

Rebohle L. , Gebel T. , von Borany J. , Skorupa W. , Helm M. , Pacifici D. , Franzo G. and Priolo F. : *Transient behavior of the strong violet electroluminescence of Ge-implanted SiO_2 layers*, Appl. Phys. B 74 (2002a) 53.

Riemann T. , Christen J. , Kaschner A. , Laades A. , Hoffmann A. , Thomsen C, Iwaya M., Kamiyama S. , Amano H. and Akasaki I. : *Direct observation of Ga-rich microdomains in crack-free AlGaN grown on patterned GaN/sapphire substrates*, Appl. Phys. Lett. 80 (2002) 3093.

Rinnert H. and Vergnat M. : *Structure and optical properties of amorphous silicon oxide films with different porosities*, J. Non-Cryst. Solids 320 (2003) 64.

Rodt S. , Seguin R. , Schliwa A. , Pötschke K. and Bimberg D. : International Conference on Luminescence ICL-05, Beijing, July 25-29, (2005), Book of Abstracts: WED-P-E-01.

Rolfe J. : *First excited state of the O^-_2* , J. Chem. Phys. 70 (1979) 2463.

Salh R. , von Czarnowski A. and Fitting H.-J. : *Multiplet luminescence of sulfur implanted silica-SiO_2:S*, phys. stat. sol.(a) 202 (2005) R53.

Schweigert I. V. , Lehtinen K. E. J. , Carrier M. J. and Zachariah M. R. : *Structure and properties of silica nanoclusters at high temperatures*, Phys. Rev. B 65 (2002) 235410.

Siu G. G. , Wu X. L. , Gu Y. and Bao X. M. : *Ultraviolet and blue emission from crystalline SiO_2 coated with $LiNbO_3$ and $LiTaO_3$*, Appl. Phys. Lett. 74 (1999) 1812.

Skuja L. N., Silin A. R. and Mares J. : *Decay time and properties of luminescence centers in vitreous silica*, phys. stat. sol (a) 50 (1978) 149.

Skuja L. : *Isoelectronic series of twofold coordinated Si, Ge, and Sn atoms in glassy SiO_2: a luminescence study*, J. Non-Cryst. Solids 149 (1992a) 77.

Skuja L. : *The origin of the 1.9eV luminescence band in glassy SiO_2*, J. Non-Cryst. Solids 179 (1994a) 51.

Skuja L. : *Direct singlet-to-triplet optical absorption and luminescence excitation band of the twofold-coordinated silicon center in oxygen-deficient glassy SiO_2*, J. Non-Cryst. Solids 167 (1994b) 229.

Skuja L. : *Optically active oxygen-deficiency-related centers in amorphous silicon dioxide*, J. Non-Cryst. Solids 239 (1998) 16.

Skuja L. , Hirano M. , Kajihara K. and Hosono H. : *Point defect creation by photochemical processes in glassy silica*, Phys. Chem. Glasses 43C (2002) 145.

Stevens-Kalceff M. A. : *Cathodoluminescence microcharacterization of the defect structure of irradiated hydratedand anhydrous fused silicon dioxide*, Phys. Rev. B 57 (1998) 5674.

Tandon P. : *Chemical annealing of oxygen hole centers in bulk glasses*, J. Non-Cryst. Solids 336 (2004) 212.

Torchynska T.V. : *Photoluminescence of Si nanocrystallites in different types of matrices*, J. Non-Cryst. Solids 352 (2006) 2484.

Trukhin A. N. : Self-*trapped exciton luminescence in α-quartz*, Nucl. Instr. and Meth. in Phys. Res. B 91 (1994) 334.

Trukhin A. N. , Goldberg M. , Jansons J. , Fitting H.-J. and Tale I. A. : *Silicon dioxide thin film luminescence in comparison with bulk silica*, J. Non-Cryst. Solids 223 (1998) 114.

Trukhin A. N. and Fitting H.-J. : *Investigation of optical and radiation properties of oxygen deficient silica glasses*, J. Non-Cryst. Solids 248 (1999) 49.

Trukhin A. N. , Fitting H.-J. , Barfels T. and von Czarnowski A. : *Cathodoluminescence and IR absorption of oxygen deficient silica-Influence of hydrogen treatment*, J. Non-Cryst. Solids 260 (1999) 132.

Trukhin A. N. , Jansons J. , Fitting H.-J. , Barfels T. and Schmidt B. : *Cathodoluminescence decay kinetics in Ge+, Si+, O+ implanted SiO2 layers*, J. Non-Cryst. Solids 331 (2003a) 91.

Tsu D. V. , Lucovsky G. and Davidson B. N. : *Effects of the nearest neighbors and the alloy matrix on SiH stretching vibrations in the amorphous SiOr:H (0<r<2) alloy system*, Phys. Rev. B 40 (1989) 1795.

Wilkinson A. R. and Elliman R. G. : *The effect of annealing environment on the luminescence of silicon nanocrystals in silica*, J. Appl. Phys. 96 (2004) 4018.

Wu X. , Zou B. , Xu J. , Yu B. , Tang G. , Zhang G. and Chen W., Nanostruct. Mat. 8 (1997) 179.

Xu Q. , Sharp I.D. , Liao C.Y. , Yi D. O. , Ager III J. W. , Beeman J. W. , Yu K. M. , Chrzan D. C. and Haller E. E. : *Germanium Nanocrystals Embedded in Sapphire*, Lawrence Berkeley National Laboratory, University of California, Paper LBNL-57463, (2005).

Yao B. , Shi H. , Zhang X. and Zhang L. : *Ultraviolet photoluminescence from nonbridging oxygen hole centers in porous silica*, Appl. Phys. Lett. 78 (2001) 174.

Yi L. X. , Heitmann J. , Scholz R. and Zacharias M. : *Phase separation of thin SiO layers in amorphous SiO/SiO2 superlattice during annealing*, J. Phys. : Condens. Matter 15 (2003) S2887.

Yu Y. H. , Wong S. P. and Wilson I. H. : *Visible Photoluminescencein Carbon-Implanted Thermal SiO2 Films*, phys. stat. sol. (a) 168 (1998) 531.

Zacharias M. , Heitmann J. , Scholz R. , Kahler U. , Schmidt M. and Bläsing J. : *Size-controlled highly luminescent silicon nanocrystals: A SiO/SiO2 superlattice approach*, Appl. Phys. Lett. 80 (2002) 661.

Zacharias M. , Yi L. X. , Heitmann J. , Scholz R. , Reiche M. and Gösele U. : *Size-controlled Si nanocrystals for photonic and electronic applications*, Solis State Phenomena 94 (2003) 95.

Zavorotny Yu. S. , Lutsko E. V. , Rybaltovskii A. O. , Chernov P. V. , Sokolov V. O. and Khrapko R. R. : *Color Centers in Sulfur-Doped Silica Glass: Spectroscopic Manifestations of an Interstitial Molecule S2*, Glass Physics and Chemistry 27 (2001) 331.

Zhang Q. , Bayliss S. C. and Frentrup W. : *The stable blue and unstable UV photoluminescence from carbon nanoclusters embedded in SiO2 matrices*, Solid State Commun. 99 (1996) 883.

Zhao J. , Mao D. S. , Lin Z. X. , Jiang B. Y. , Yu Y. H. , Liu X. H. , Wang H. Z. and Yang G. Q. : *Intense short-wavelength photoluminescence from thermal SiO2 films co-implanted with Si and C ions*, Appl. Phys. Lett. 73 (1998) 1838.

Zorenko Y. , Gorbenko V. , Voloshinovskii A. , Stryganyuk G. , Nedilko S. , Degoda V. and Chukova O. : *Luminescence of Sc-related centers in single crystalline films of Lu3Al5O12 garnet*, phys. stat. sol. (c) 2 (2005) 105.
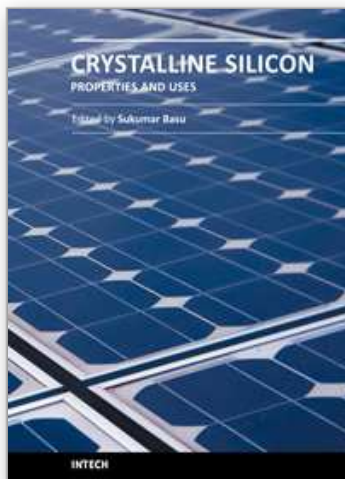
Crystalline Silicon - Properties and Uses

Edited by Prof. Sukumar Basu

The exciting world of crystalline silicon is the source of the spectacular advancement of discrete electronic devices and solar cells. The exploitation of ever changing properties of crystalline silicon with dimensional transformation may indicate more innovative silicon based technologies in near future. For example, the discovery of nanocrystalline silicon has largely overcome the obstacles of using silicon as optoelectronic material. The further research and development is necessary to find out the treasures hidden within this material. The book presents different forms of silicon material, their preparation and properties. The modern techniques to study the surface and interface defect states, dislocations, and so on, in different crystalline forms have been highlighted in this book. This book presents basic and applied aspects of different crystalline forms of silicon in wide range of information from materials to devices.

INTECH
open science | open minds